https://doi.org/10.5194/cp-2021-18
Preprint. Discussion started: 11 March 2021

Maastrichtian-Rupelian paleoclimates in the southwest Pacific – a critical evaluation of biomarker paleothermometry and dinoflagellate cyst paleoecology at Ocean Drilling Program Site 1172

Peter K. Bijl[1]*, Joost Frieling[1,2], Margot J. Cramwinckel[1,3], Christine Boschman[1], Appy Sluijs[1], Francien Peterse[1]

[1]Department of Earth Sciences, Utrecht University, Utrecht, the Netherlands.
[2]now at: Department of earth Sciences, University of Oxford, South Parks Road OX1 3AN, UK
[3]now at: School of Ocean and Earth Science, National Oceanography Centre Southampton, University of Southampton, Southampton, UK

* corresponding author. email: p.k.bijl@uu.nl

Abstract

Sea surface temperature (SST) reconstructions based on isoprenoid glycerol dialkyl glycerol tetraether (isoGDGT) distributions from the Eocene southwest (sw) Pacific Ocean are unequivocally warmer than can be reconciled with state-of-the-art fully coupled climate models. However, the SST signal preserved in sedimentary archives can be affected by contributions of additional isoGDGT sources. Methods now exist to identify and possibly correct for overprinting effects on the isoGDGT distribution in marine sediments. We here use the current proxy insights to assess the reliability of the isoGDGT-based SST signal in 69 newly analysed and 242 re-analysed sediments ODP Site 1172 (East Tasman Plateau, Australia) following state-of-the-art chromatographic techniques, in context of paleo-environmental and paleoclimatologic reconstructions based on dinoflagellate cysts. The resulting ~130 kyr-resolution Maastrichtian-Oligocene TEX_{86}-based SST record confirms previous conclusions of anomalous warmth in the early Eocene sw Pacific and remarkably cool conditions during the mid-Paleocene. Dinocyst diversity and assemblages show a strong response to the local SST evolution, supporting the robustness of the TEX_{86} record.

Soil-derived branched GDGTs stored in the same sediments are used to reconstruct mean annual air temperature (MAAT) of the nearby land using the MBT'$_{5me}$ proxy. MAAT is consistently lower than SST during the early Eocene, independent of the calibration chosen. General trends in SST and MAAT are similar, except for: 1) an enigmatic absence of MAAT rise during the Paleocene-Eocene Thermal Maximum and Middle Eocene Climatic Optimum, and 2) a subdued middle–late Eocene MAAT cooling relative to SST. Both dinocysts and GDGT signals suggest a mid-shelf depositional environment with strong river-runoff during the Paleocene-early Eocene, progressively becoming more marine thereafter. This trend reflects gradual drying and more pronounced wet/dry seasons in the northward drifting Australian hinterland, which may also explain the subdued middle Eocene MAAT cooling relative to that of SST. The overall correlation between dinocyst assemblages, marine biodiversity and SST changes suggests that temperature exerted a strong influence on the surface-water ecosystem, probably in part through sea level changes caused by steric effects. Finally, we find support for a potential temperature control on compositional changes of branched glycerol monoalkyl glycerol tetraethers (brGMGTs) in marine sediments. It is encouraging that a critical evaluation of the GDGT signals confirms the vast majority of the generated data is reliable. However, this also implies the high TEX$_{86}$-based SSTs for the Eocene sw Pacific, and the systematic offset between absolute TEX$_{86}$-based SST and MBT'$_{5me}$-based MAAT estimates remain unexplained.

1. Introduction

1.1 The Paleogene Southwest Pacific Ocean

Reconstructions of deep-sea (Westerhold et al., 2020) and sea surface temperature (Bijl et al., 2009; 2013a; Cramwinckel et al., 2018; Frieling et al., 2014; Hollis et al., 2014; 2019; Inglis et al., 2015; 2020; O'Brien et al., 2017; Evans et al., 2018; O'Connor et al., 2019; Sluijs et al., 2020) have revealed overall cool climate in the Maastrichtian and Paleocene, long-term warming towards the early Eocene Climatic Optimum (EECO; 53.4 – 49.2 Ma), and subsequent cooling during the middle and late Eocene (48.6 – 33.6 Ma). The EECO stands out as particularly warm, with ice-free polar regions (Bijl et al., 2013a; Hines et al., 2017; Pross et al., 2012; Frieling et al., 2014). Certain southern high-latitude regions retain warm-temperate conditions into the late Eocene (Bijl et al., 2009; Houben et al., 2019) and, despite ample evidence for pronounced Antarctic glacial expansion across the Eocene-Oligocene transition (Salamy and Zachos, 1999; Bohaty et al., 2012), even into the early Oligocene (Hartman et al., 2018; Passchier et al., 2013; 2017; O'Brien et al., 2020). Variations in atmospheric CO_2 concentrations (Beerling and Royer, 2011; Anagnostou et al., 2016; Foster et al., 2017) are likely the primary driver of these multi-million-year climatic trends (Cramwinckel et al., 2018). While equatorial proxy-based sea surface temperatures (SSTs) and deep-sea temperatures, assumed to reflect high-latitude SSTs, show good correspondence with numerical model simulations under Eocene boundary conditions and with varying CO_2 forcing (Cramwinckel et al., 2018), proxy-based SST reconstructions of the southwest (sw) Pacific remain warmer than those from model simulations (Bijl et al., 2009; Cramwinckel et al., 2018; Hollis et al., 2012; Lunt et al., 2021), despite proposed zonal heterogeneity (Douglas et al., 2014). Specifically, numerical models are currently unable to simulate a paleoclimate in which the annual SST difference between the equatorial Atlantic Ocean (Cramwinckel et al. 2018) and the sw Pacific Ocean (Bijl et al., 2013a; Hollis et al., 2012) is as small as the proxy data suggests. Without this model-data mismatch resolved, it remains unclear to what extent numerical models properly simulate polar amplification of Paleogene climates and if the current proxies properly reflect high latitude temperatures under greenhouse conditions (Lunt et al., 2012).

https://doi.org/10.5194/cp-2021-18
Preprint. Discussion started: 11 March 2021

Proxy evidence for warmth in the Eocene sw Pacific region derives from a suite of organic and calcite-based proxies. In terms of the latter, oxygen isotope ratios ($\delta^{18}O$) and trace element ratios (Mg/Ca) from well-preserved planktonic foraminifera indicate warm temperatures from Eocene sections in New Zealand (Creech et al., 2010; Hines et al., 2017; Hollis et al., 2009; 2012). These proxies require assumptions regarding seawater chemistry (Mg/Ca, $\delta^{18}O$ seawater, pH) that carry significant uncertainty (e.g., Kozdon et al., 2020, Evans et al. 2018). The application of clumped isotope paleothermometry has great potential to partially alleviate such concerns, as evident from work on Seymour Island (Douglas et al., 2014). Pollen-based vegetation reconstructions from New Zealand, the Tasman region and Wilkes Land (Carpenter et al., 2012; Contreras et al., 2013; 2014; Huurdeman et al., 2020; Pross et al., 2012), however, confirm warm conditions, and arguably deliver the best constraints on winter temperatures. This is because of fundamental physiological restrictions in their individual tolerances (e.g., Reichgelt et al., 2018), whereas mean annual air temperature (MAAT) reconstructions from pollen assemblages are complicated because MAAT exerts much less control on the standing vegetation than seasonal temperature and hydrological extremes. Reconstructions of the warm Eocene primarily relied on organic geochemical proxies, notably TEX_{86} (Bijl et al., 2009; 2013a; Cramwinckel et al., 2018; 2020; Crouch et al., 2020; Hollis et al., 2009; 2012; Sluijs et al., 2006; 2009; 2011). These absolute SST estimates for the sw Pacific are closer to those from the equatorial Atlantic as they are to the deep-sea (Cramwinckel et al., 2018), which is surprising given that the South Pacific was presumably the dominant region of deep-water formation during the Eocene (Huber and Thomas, 2010; Thomas et al., 2003; 2014).

1.2 GDGT paleothermometry

TEX_{86} utilizes the correspondence of higher abundances of cyclopentane rings in sedimentary archaeal membrane lipids termed isoprenoid glycerol dialkyl glycerol tetraethers (isoGDGTs) with higher SST of the overlying surface water (Schouten et al., 2002). This relation is attributed to a viscoelastic adaptation of the membrane of pelagic Thaumarcheota, the dominant source organisms of isoGDGTs, to temperature (Schouten et al., 2002; 2013). For some periods in geological deep time, including the

Paleocene and Eocene, TEX_{86} calibrations based on GDGTs in core top sediments need to be extrapolated above the modern SST range (~30°C) to estimate SST. The linearity of the relation at and beyond the high-end of the core-top calibration is poorly known, leading to very high uncertainty in SST estimates at the warm end of the calibration (Hollis et al., 2019). However, as the absolute TEX_{86} values of many Eocene sediments exceed those observed for modern core-tops, even the most conservative calibrations yield SSTs >30°C in the warmest intervals. Increasingly, such temperatures are corroborated by estimates from other SST proxies (e.g., Zachos et al, 2006; Frieling et al., 2017; Evans et al., 2018).

Along with calibration uncertainties, a number of confounding factors have been identified since first publication of the isoGDGT-based SST records from the sw Pacific (Hollis et al., 2009; 2012; Bijl et al., 2009; 2013), relating to a suite of pre-, syn-, and post-depositional processes that might alter the pelagic isoGDGT signal in marine sediments. IsoGDGT contributions from methanogenic (Blaga et al., 2009) and methanotrophic (Weijers et al., 2011; Zhang et al., 2011) archaea, deep-dwelling archaea (Taylor et al., 2013) and terrestrial sources (Hopmans et al., 2004; Weijers et al., 2006) to the sedimentary isoGDGT pool have been determined. These factors can be recognized in GDGT distributions, leading to better interpretation of TEX_{86}–based SST reconstructions. However, the influence of growth phase (Elling et al., 2014), and environmental ammonium and oxygen concentrations (Qin et al., 2015; Hurley et al., 2016) on sedimentary isoGDGT distributions are as yet poorly constrained.

Branched GDGTs (brGDGTs) produced by soil bacteria provide reconstructions of mean annual air temperature (MAAT) using the MBT'_{5me} index (De Jonge et al., 2014a; Naafs et al., 2019; Peterse et al., 2012; Weijers et al., 2007; Dearing Crampton-Flood et al., 2020). Based on brGDGTs supplied to marine sediments, the MAAT evolution of Australian-New Zealand continents followed the trends in deep- and surface ocean temperature remarkably well, but with much lower absolute values than SST (Bijl et al., 2013a; Pancost et al., 2013). Albeit to a lesser extent than SST, southern high-latitude MAAT reconstructions remain warmer than model simulations (Huber and Caballero, 2011) as well, even when simulations replicate equatorial surface and global deep ocean temperatures (Cramwinckel et al., 2018). With improved analytical techniques (Hopmans et al., 2016), brGDGT isomers with a methylation on the 5- or the 6-position of the alkyl chain can now be separated and quantified (De Jonge et al., 2013). With this separation, the pH co-dependence of the brGDGT signal can be removed, isolating the temperature relation (De Jonge et al., 2014a; Naafs et al., 2017a). The separation of brGDGT isomers also allows to recognize and correct for potential contributions of aquatic brGDGTs to the soil-derived brGDGT signal stored in marine sediments that complicate the use of brGDGTs as continental paleothermometer in continental margin sediments (De Jonge et al., 2014b; 2015; Dearing Crampton-Flood et al., 2018; Peterse et al., 2009; Sinninghe Damsté, 2016; Tierney and Russell, 2009; Zell et al., 2013).

Lipids from a related biomarker family, the branched glycerol monoalkyl glycerol tetraethers (brGMGTs), were identified in the marine realm in core-top sediments (Liu et al., 2012), oxygen minimum zones (Xie et al. 2014), and later in peat (Naafs et al 2018a) and East African lake sediments (Baxter et al 2019), the latter identifying 7 individual brGMGTs. The brGMGTs contain a covalent bond connecting the two alkyl chains. The abundance of brGMGTs relative to that of brGDGTs, as well as the relative distribution of brGMGT isomers seems to vary with temperature in some degree (Baxter et al., 2019; Naafs et al., 2018a; Tang et al., 2021), although this is thus far only based on empirical relationships. The exact sources of these compounds, and consistency of such signals in various terrestrial, lacustrine and marine realms, are as yet not fully understood. The degree of methylation of a specific subset of brGMGT compounds (Naafs et al., 2018a, Sluijs et al. 2020) is however similar to those in brGDGTs for which membrane stability regulation is proposed as underlying mechanism (Weijers et al., 2007). Paleogene marine sediments from the Arctic Ocean do contain abundant brGMGTs (Sluijs et al., 2020), and these seem to be produced in the marine system with a strong oxygen minimum zone, and substantial terrestrial input. While the degree of methylation of acyclic brGMGTs ($\mathrm{HMBT}_{\mathrm{acyclic}}$) does show similar trends to TEX_{86} in the Paleogene Arctic record, brGMGTI, which was tentatively calibrated to temperature using a suite of tropical lakes (Baxter et al., 2019) does not (Sluijs et al., 2020). The response of brGMGTs to environmental and climatic changes, as well as their sourcing in the marine realm, is clearly diverse, complex and, as yet, poorly understood.

1.3 Revisiting GDGTs, and investigating GMGTs at Site 1172

From the new insights about the GDGT-based proxies, it is clear that assessing the reliability of previously published GDGT-based temperature reconstructions requires a revisit and a detailed constraints on past environmental, climatological and depositional conditions. Moreover, the presence and proxy potential of brGMGTs the early Paleogene sw Pacific has not yet been assessed. To this end, we have revisited a sedimentary record from the sw Pacific Ocean: ODP Site 1172 on the East Tasman Plateau (ETP), which contains an almost complete succession of late Cretaceous to early Oligocene sediments (Bijl et al., 2013b; 2014; Brinkhuis et al., 2003; Schellenberg et al., 2004; Stickley et al., 2004a). We have newly analysed isoGDGTs, brGDGTs, and brGMGTs from the Maastrichtian and Paleocene section of the record, and re-analysed previously published sample sets using the chromatography method with improved compound separation (Hopmans et al., 2016). We critically evaluate the biomarker results using established indicators for pre-, syn- or post-depositional overprint of the primary sea surface and air temperature signals. In addition, we use dinoflagellate cyst assemblages and terrestrial palynomorph abundance as recorders of paleoenvironmental change on the continental shelf, for constraints on depositional, environmental and hydrological changes, in order to aid interpretations of the GDGT indices. We also evaluate the nature, source and possible temperature affinity of the brGMGTs in our record. After this critical (re-)evaluation, we interpret the Maastrichtian to early Oligocene sea surface and air temperature, and paleoenvironmental evolution of the sw Pacific region.

Fig. 1

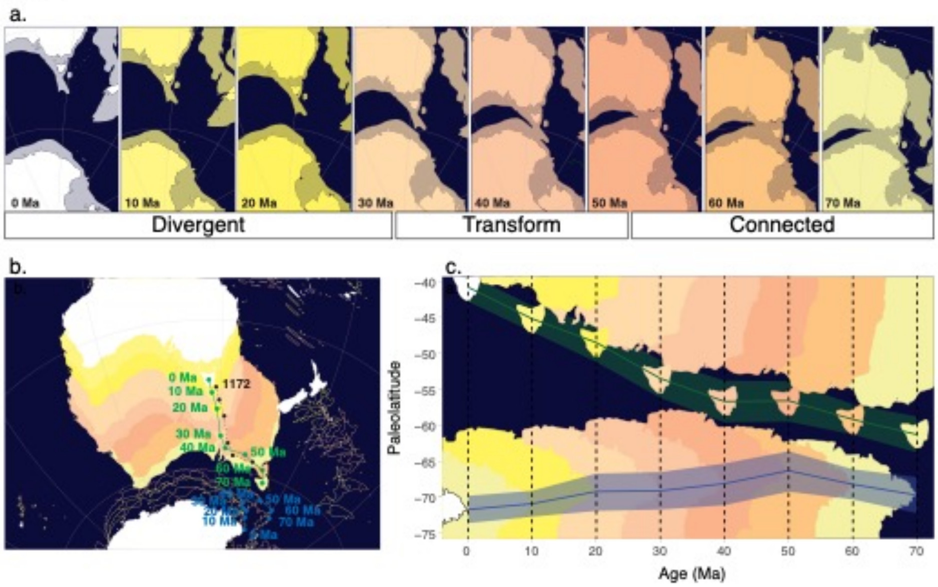

Figure 1. Absolute plate tectonic changes around Tasmania during the Maastrichtian to recent. a. TG opening in 8 time slices, from 70 Ma to present. Relative tectonic motion between Australia and Antarctica is limited until about 53 Ma, transfer until 34 Ma and divergent from 34 Ma onwards. b. Like a, but on an orthographic projection (compiled with Gplates, using paleomagnetic reference frame (Torsvik et al., 2012) from Seton et al. (2012)). Green and blue lines and dots represent the pathways of Tasmania and Cape Adare, respectively, black dashed line and dots represent the paleo-position of Site 1172. c. The absolute paleolatitude of Cape Adare, Antarctica (blue line, blue shading = uncertainty), as indicative of the plate tectonic motion around the pathway of the Tasman Current, and of Tasmania (green line, green shading = uncertainty), as indicative of the plate tectonic motion of the source area of the terrestrial organic matter, in 10 Myr time steps from 70–0 Ma. obtained from paleolatitude.org (Van Hinsbergen et al., 2015). Plate contours represent paleolatitude of present-day shorelines, for orientation (obtained from Gplates). Note that in visualizations b and c, submerged continental crust is not shown, but does limit TG opening.

2. Material

2.1 Site locality and tectonic evolution

Since the Cenomanian, the continental complex including Australia, Tasmania, ETP and the South Tasman Rise (STR) tectonically moved as one continental plate (Müller et al., 2000) – here referred to as Australia. True polar wander, although relatively poorly constrained, has caused absolute plate motions relative to the spin axis of the Earth (Torsvik et al., 2012; Van Hinsbergen et al., 2015). On a paleomagnetic reference frame, Antarctica and Australia rotated northwestward by 3° of latitude and over 3° longitude between 70 and 50 Ma (Fig. 1), with only little transform displacement between them. From 50 Ma onwards, the tectonic drift orientation of Antarctica shifted slightly more southwards than that of Australia, causing left transform motion between notably west of Cape Adare and west Tasmania (Fig. 1; Williams et al., 2019). Although this divergence effectively opened the Tasmanian Gateway (TG) to surface flow of the Antarctic Counter Current close to the early-middle Eocene boundary (Bijl et al., 2013a), probably through subsidence of the Antarctic continental margin and STR, rapid northward movement of Australia and southward movement of East Antarctica did not start before about 40 Ma (Fig. 1; Cande and Stock, 2004; Seton et al., 2012). Yet, a connection between Australian and Antarctic continental blocks persisted until 34Ma when transform motion between STR and Wilkes Land changed into spreading and ocean crust formation (Cande and Stock, 2004; Seton et al., 2012).

Fig. 2

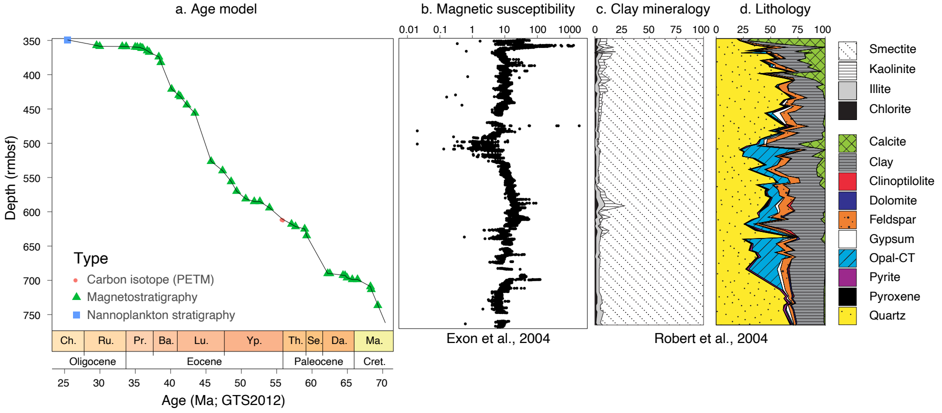

Figure 2. a. Age tie points used to construct the age model for ODP Site 1172, based on carbon isotope (Bijl et al., 2010; Sluijs et al., 2011), magnetostratigraphic (Bijl et al., 2010; Houben et al., 2019; Stickley et al., 2004a), and nannofossil (Houben et al., 2019) age constraints. b. Shipboard magnetic susceptibility from Exon et al. (2001). c. Shore-based clay mineralogy and d. smear slide-based lithological observations from Robert (2004).

2.2 Lithology

A 760 meter thick sediment sequence was recovered at ODP Site 1172, on the western part of the ETP, east of Tasmania, Australia (Exon et al., 2001). We studied the interval from 760 meters below sea floor (mbsf) to about 350 mbsf in a composite (Röhl et al., 2004a) of Hole A and D. The carbonate ooze from 350 mbsf upwards did not yield any GDGTs. The studied succession consists broadly of green-grey silty claystones from 760 to ~505 mbsf, grading into dark grey to black silty claystones from 636 – 625 mbsf, then a return of the greenish grey silty claystones, which is interrupted by a more lithified unit at 610 mbsf (Exon et al., 2001; Röhl et al., 2004a, b; Schellenberg et al., 2004; Sluijs et al., 2011). The silty claystones turn gradually and cyclically lighter from 570 mbsf upwards until ~361 mbsf, with gradually more calcium carbonate and diatoms preserved (Röhl et al., 2004a). The clay mineralogy is dominated by smectite but contains progressively more kaolinite above ~500 mbsf (Fig. 2; Exon et al., 2001; Robert, 2004). Grey silty claystones give way to a green glauconitic horizon between 360.1 and 357.3 mbfs (Exon et al., 2001). Above this greensand, carbonate oozes continue further upwards. The record is quasi-continuously bioturbated by zoophycos (Exon et al., 2001). We follow the depth corrections published in (Sluijs et al., 2011) for Cores 12R–31R, based on the correlation of core-log and downhole log magnetic susceptibility.

2.3 Age model

For age tie points (Table S1; Fig. 2), we use the identification of the PETM (Sluijs et al., 2011) and Middle Eocene Climatic Optimum (MECO; Bijl et al., 2010) and robust biostratigraphical constraints from the Eocene–Oligocene Boundary interval

(Houben et al., 2019; Sluijs et al., 2003). In the intervals in between, the age model relies on magnetostratigraphy, which in some intervals suffers from a strong normal overprint (Dallanave et al., 2016), calibrated using nannofossil- diatom- and dinocyst biostratigraphy (Bijl et al., 2013b; Stickley et al., 2004). Despite the overprint, there does seem to be a paleomagnetic signal preserved in the inclination data (Fuller and Touchard, 2004), and biostratigraphic constraints are broadly consistent with nearby sites (Bijl et al., 2013b; Dallanave et al., 2016).

The nature of the sediments and depositional setting (see below) implies that small hiatuses may exist between the age tie points (Röhl et al., 2004a). Indeed, hiatuses were already identified across the Cretaceous–Paleogene Boundary (Schellenberg et al., 2004), in the mid-Paleocene (Bijl et al., 2013b; Hollis et al., 2014), early Eocene (Bijl et al., 2013b) and in the middle Eocene (Röhl et al., 2004a), corresponding to increases in magnetic susceptibility (Fig. 2). The section across the Eocene–Oligocene transition is strongly condensed (Houben et al., 2019; Stickley et al., 2004a, b).

2.4 Depositional setting

From the lithology (Robert, 2004) and palynological content (Brinkhuis et al., 2003), the Maastrichtian–Eocene part of the record was interpreted to represent a shallow-marine, mid-continental shelf depositional setting, with gradual deepening in the middle Eocene based on an increase in calcium carbonate content (Fig. 2; Röhl et al., 2004a). The late Eocene greensands have been initially interpreted as evidencing strong deepening and current inception as a result of widening of the TG (Stickley et al., 2004b). Later studies have related the greensands to invigorated ocean circulation and winnowing (Houben et al., 2019), and not necessarily deepening of the site. Volcanic activity of the Balleny plume in the late Eocene (Hill and Moore, 2001) might have played a profound role in the bathymetric changes of the ETP, in addition to the tectonic stresses that act on diverging plates in the TG area.

The regional tectonic evolution has implications for interpreting the marine and terrestrial temperature record at this site, because it influenced regional oceanography and climatic conditions in the hinterland catchment area. Field data and model simulations indicate that with a closed TG, the Tasman Current, a strong western boundary current of the proto-Ross gyre, bathed the plateau with Antarctic-derived surface waters (Bijl et al., 2011; 2013b; Huber et al., 2004; Sijp et al., 2014; 2016). Palynological evidence confirms that the Proto-Ross Gyre influence persisted at the ETP until the late Eocene (Bijl et al., 2011; Warnaar et al., 2009). This means that despite northward tectonic drift, the same strong western boundary current bathed the site during the Maastrichtian to early Eocene (Sijp et al., 2016), with perhaps some intermittent influence of East Australian Current waters from the north (Bijl et al., 2010; Cramwinckel et al., 2020). This ended when the proto-Leeuwin Current started to flow through the progressively widening TG (Fig. 1), bringing the ETP under the influence of more northerly sourced surface waters (Houben et al., 2019; Stickley et al., 2004b).

The source area for the terrestrial organic matter (OM) and detrital input was likely Tasmania. Persistent terrigenous input (Brinkhuis et al., 2003) arguably requires a large terrestrial catchment area, and the ETP seems too small (~50,000 km^2) to have had vast areas above sea level. Moreover, Paleocene–Eocene terrestrial palynomorph assemblages contain common Permian–Triassic elements (Contreras et al., 2014); the Permian–Triassic upper Parmeener group contains thick terrestrial (coal) deposits and comprises the surface lithology of most of eastern Tasmania today. Although that same formation might be present in the ETP subsurface as well, it was probably covered with sediment throughout the Cenozoic (Hill and Moore, 2001). Rivers flowing from southeast Australia drained into the Gippsland and Bass Basins, and that terrigenous material is unlikely to have reached the ETP. Seismic information from the East Tasman Saddle, connecting the Tasmanian Margin to the ETP, does not suggest there was a deep basin in between (Hill and Exon, 2004). Therefore, Tasmanian-sourced detrital material could reach the ETP. The ETP was close enough to the Antarctic margin during the Maastrichtian–early Eocene to have received perhaps a minor component of Antarctic-sourced terrestrial OM input, in addition to the dominant Tasmanian source. The regional palynology (Macphail, 2000; 2002; Carpenter et al., 2012; Pross et al., 2012; Contreras et al., 2013; 2014; Truswell, 1997), the abundance of peatlands (Holdgate et al., 2009), and the felsic lithology (Moore, Betts, and Hall, 2013) suggests the hinterland catchment contained acidic, wet soils and peats.

2.5 Samples

For this study, we used lipid extracts that have been analysed for GDGTs previously (Bijl et al., 2009; Hollis et al., 2014; Houben et al., 2019; Sluijs et al., 2011). We augmented these with 69 new extracts of sediments from the Maastrichtian and the Paleocene, to extend and improve the temporal resolution of the record. Unfortunately, not all archived samples from the PETM interval (Sluijs et al., 2011) could be located, and the interval was reanalysed in a lower resolution (6 samples over the PETM interval). For the remaining PETM, we used the published peak areas (Sluijs et al., 2011) to calculate TEX_{86}, which is warranted given the new analytical technique does not affect isoGDGT peak area ratios (Hopmans et al., 2016). For palynology, we collated and revisited data presented in (Bijl et al., 2010; 2013b; Brinkhuis et al., 2003; Houben et al., 2019; Sluijs et al., 2011) and generated higher-resolution data for the Maastrichtian and Paleocene.

3. Methods

3.1 Organic geochemistry

3.1.1 Extraction, column separation and analysis

Earlier work (Bijl et al., 2009; 2010; 2013a; Houben et al., 2019; Sluijs et al., 2011) presented in detail the extraction, Al_2O_x column separation and filtering techniques used for the samples. We followed the same procedures for the processing of the new samples. We reanalysed all available polar fractions using the double column UHPLC-MS approach as described in (Hopmans et al., 2016). In short, processing involved extraction with a Dionex accelerated solvent extractor using dichloromethane:methanol (DCM:MeOH) 9:1 (v/v), column separation of the total lipid extract using solvent mixtures hexane:DCM 9:1 (v/v), hexane:DCM 1:1 (v/v) and DCM:MeOH 1:1 (v/v) for apolar, ketone and polar fractions, respectively. Polar fractions were filtered using a 0.45 μm polytetrafluorethylene filter, and analysed using an Agilent 1260 Infinity series HPLC system coupled to an Agilent 6130 single-quadrupole mass spectrometer.

3.1.2 Data analysis: indices, overprints

Since the discovery of isoGDGTs as proxy for SST (see Schouten et al. (2013) for a review), several non-SST effects have been identified that may affect the distribution of isoGDGTs in the sediment. Several indices have been developed to identify most of the known sources of overprints (Table 1). Next to signalling SST-unrelated influences on the isoGDGT pool, these indices also provide information on the prevailing marine and paleoenvironmental and depositional conditions.

Table 1: Indices from iso- and brGDGTs and brGMGTs. For the chemical structure of these components see Fig. 3.

Index name	**Equation**	**Proxy for**	**Cut-off value**	**Source**
TEX_{86}	$\frac{GDGT2 + GDGT3 + Cren'}{GDGT1 + GDGT2 + GDGT3 + Cren'}$	Sea surface temperature	-	(Schouten et al., 2002)
BIT index	$\frac{IIIa + IIIa' + IIa + IIa' + Ia}{Cren + IIIa + IIIa' + IIa + IIa' + Ia}$	Terrestrial input	>0.4? Site-dependent	(Hopmans et al., 2004)
fcren’	$\frac{\%Cren^{\backprime}}{\%Cren^{\backprime} + \%Cren}$	Non-thermal contribution of crenarchaeol isomer	0.25	(O'Brien et al., 2017)
Methane Index	$\frac{GDGT1 + GDGT2 + GDGT3}{GDGT1 + GDGT2 + GDGT3 + Cren + Cren'}$	Contribution by methane-metabolising archaea	>0.3	(Zhang et al., 2011)
AOM ratio	$GDGT2/Cren$	Contribution by anaeropbic methane oxydizers	>0.2	(Weijers et al., 2011)
GDGT2/3 ratio	$GDGT2/GDGT3$	Contribution by deep-dwelling archaea	>5	(Taylor et al., 2013)
Methano-genesis	$GDGT0/Cren$	Contribution by methanogenic archaea	>2.0	(Blaga et al., 2009)
Ring index (RI)	$0*\%GDGT0 + 1*\%GDGT1 + 2*\%GDGT2 + 3*\%GDGT3 + 4*\%Cren + 4*\%Cren'$	Non-pelagic GDGT composition	ΔRI >0.3*	(Zhang et al., 2016)
MBT'_{5me}	$\frac{IIIa + IIIb + IIIc}{IIIa + IIIb + IIIc + IIa + IIb + IIc + Ia}$	Mean annual air temperature	-	(De Jonge et al., 2014a)
CBT’	$\frac{IIIb + IIb' + IIc' + Ia'}{IIIa + IIa + Ia}$	(soil-)pH	-	(De Jonge et al., 2014a)
$\#rings_{tetra}$	$\frac{Ib + 2 * Ic}{Ia + Ib + Ic}$		>0.7	

#rings$_{penta}$	$\frac{IIb + IIb' + 2 * IIc + 2 * IIc'}{IIa + IIa' + IIb + IIb' + IIc + IIc'}$	Marine in situ brGDGT production	-	(Sinninghe Damsté, 2016)
#rings$_{penta5}$	$\frac{IIb + 2 * IIc}{IIa + IIb + IIc}$		-	
#rings$_{penta6}$	$\frac{IIb' + 2 * IIc'}{IIa' + IIb' + IIc'}$		-	
IR	$\frac{IIa' + IIb' + IIc' + Ia'}{IIa + IIa' + IIb + IIb' + IIc + IIc' + Ia + Ia'}$	River in situ brGDGT production	Depends on soil value	(De Jonge et al., 2014b)
IR$_{hexa}$	$\frac{Ia'}{Ia + Ia'}$		-	(Sinninghe Damsté, 2016)
IR$_{penta}$	$\frac{IIa' + IIb' + IIc'}{IIa + IIa' + IIb + IIb' + IIc + IIc'}$			
brGMGTI	$\frac{H1020c + H1034a + H1034c}{\mathrm{H1020b} + \mathrm{H1020c} + H1034a + H1034b + H1}$	Temperature, oxygenation?	In lakes	(Baxter et al., 2019)
%brGMGT, %brGMGT$_{a}$ cyclic	$\frac{[brGMGT]}{[brGMGT] + [brGDGT]} \times 100$		In peats, lakes	(Baxter et al., 2019)
	$\frac{[brGMGT]}{[Ia + IIa + IIIa + brGMGT]} \times 100$			(Naafs et al., 2018a)
HMBT$_{acyclic, all}$	$\frac{H1020a + H1020b + H1}{H1020a + H1020b + H1020c + H1034a + H1}$		In peats	(Naafs et al., 2018a)
HMBT$_{acyclic}$	$\frac{H1020c}{H1020c + 1034b + H1048}$		In Arctic Ocean sediments	Sluijs et al., 2020, sensu Naafs et al., 2018a)

* Cutoff depends on TEX$_{86}$ value. ΔRI = RI$_{TEX}$ – RI, where RI$_{TEX}$ = -0.77*TEX$_{86}$ + 3.32*TEX$_{86}$^2 + 1.59

Fig. 3

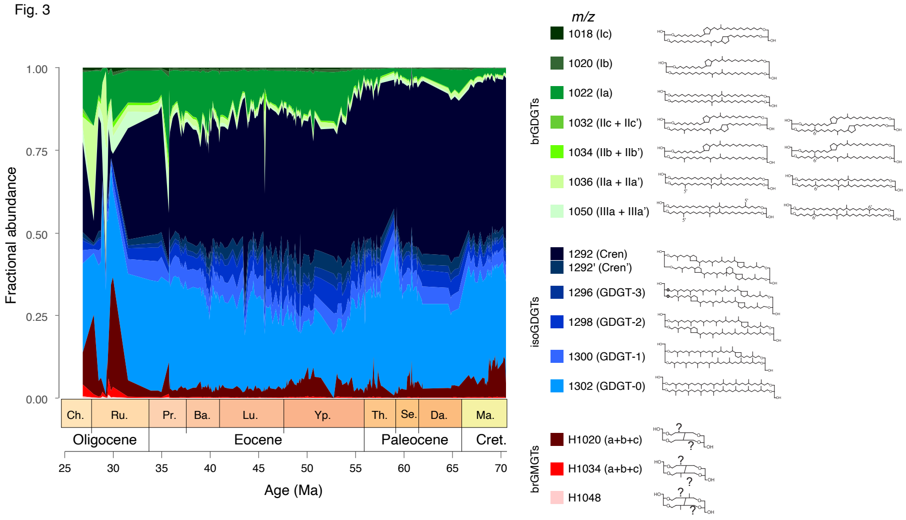

https://doi.org/10.5194/cp-2021-18
Preprint. Discussion started: 11 March 2021

Figure 3. Fractional abundances of the various branched (green) and isoprenoidal (blue) GDGTs, and branched GMGTs (red) at ODP Site 1172.

All of the ratios that signal biases express the influence of this bias relative to modern "normal" or idealized compositions. The abundance of overprinted components is divided over either a total sum of overprinted and non-overprinted components (closed sum; e.g., methane index, IR) or over only the non-overprinted (ratio; GDGT2/3 ratio, AOM ratio). The complication is that a change in index value can be caused by changes in the denominator or numerator. This is particularly evident in the interpretation of the branched and isoprenoid tetraether (BIT) index. It was proposed that the closed sum ratio between brGDGTs, which were thought to derive exclusively from soils, and the isoGDGT crenarchaeol, which was thought to be produced exclusively by marine archaea, could be an indicator for the relative contribution of soil organic matter (OM) into marine sediments (Hopmans et al., 2004). However, it was subsequently shown that crenarchaeol, but critically also other isoGDGTs are produced on land (Weijers et al. (2006), and that a large contribution of soil-OM to marine sediments can cause a bias in TEX_{86}. Weijers et al. (2006) used an end-member model to calculate the potential bias in TEX_{86}-based SST reconstructions in the Congo Fan and this shows significant bias (>2°C) for BIT above 0.3. However, it is rather arbitrary to assign a cut-off for BIT based on the magnitude of the SST bias alone, as this bias depends primarily on the difference between the isoGDGT composition of the soil and marine endmembers. As a consequence, there is no uniform cut-off value for BIT index above which TEX_{86} should be discarded. Secondly, because the BIT index is a closed sum, the index is equally affected by increased production of crenarchaeol as it is by the input of brGDGTs. Although this could be verified with absolute concentrations of GDGTs, these are not always presented. Third, brGDGTs are produced in situ in the marine realm (Dearing Crampton-Flood et al., 2019; Peterse et al., 2009; Sinninghe Damsté, 2016). The corollary of this is that the cut-off value for BIT to infer an overprint in the isoGDGT-based SST signal should be assumed to differ per environmental setting, and perhaps also through time if the setting changes majorly (e.g., Sluijs et al., 2020). As a result, cut-offs were set higher (e.g., 0.4; Bijl et al., 2013a) when no relationship between TEX_{86} and BIT index values was detected. This approach is also not without complications, because the abundance and composition of isoGDGTs (including crenarchaeol) in soil material varies (Weijers et al., 2006; De Jonge et al., 2015; De Jonge et al., 2016; Naafs et al., 2019; Sluijs et al., 2020). This in turn implies that in samples with high BIT (Weijers et al., 2006), the terrestrially-derived isoGDGT contribution will not be uniform, and might become impossible to detect in a TEX_{86}-BIT index cross plot. In some paleo-environmental settings that evidently lack high input of soil-OM, BIT index values are high (Leutert et al., 2020). For reasons given above, this could either mean very low crenarchaeol production in the marine realm, or in situ production of brGDGTs. These two scenarios make for a completely different paleoenvironmental interpretation, and fail to indicate whether the brGDGTs can be used to reconstruct MAAT of the hinterland or whether isoGDGTs can be used for reliable paleothermometry. For that, it is important to assess the sources of brGDGTs, as brGDGTs produced in rivers (De Jonge et al., 2014b; Zell et al., 2013) or the (coastal) marine environment (Dearing Crampton-Flood et al., 2019; Peterse et al., 2009; Sinninghe Damsté, 2016) may contribute and thereby bias the initial soil-derived brGDGT signal, affecting the reliability of MAAT reconstructions. Fortunately, production of brGDGTs in the marine realm can be recognized based on the weighed number of rings of the tetramethylated brGDGTs, quantified in the $\#rings_{tetra}$, where values >0.7 indicate a purely marine source of the brGDGTs (Sinninghe Damsté, 2016). Similarly, brGDGTs that are produced in rivers are characterized by a relatively high abundance of the 6-methyl brGDGTs relative to the 5-methyl brGDGTs, expressed as the Isomerization Ratio (IR; De Jonge et al., 2014b).

For the other overprinting indices, cut-off values may not be as uniformly applicable to all depositional settings either. Leutert et al. (2020) showed that modern samples exceeding cut-off values for the GDGT2/3 ratio and methanogenesis index do not have anomalous TEX_{86} index values in the modern core-top dataset based on the Ring index. This suggests that the TEX_{86} index value is not equally influenced by non-thermal contributions in all depositional settings. As a result, evaluating non-thermal contributions on TEX_{86} index values should consider the depositional and environmental setting along with the cut-off values.

3.1.3 Calibrations for TEX$_{86}$ and MBT'$_{5me}$

An extensive number of calibrations has been proposed to convert TEX$_{86}$ index values to sea surface temperatures. At the heart of the calibration discussion is the uncertainty whether the TEX$_{86}$-to-SST relationship continues in a linear way beyond the modern SST range, or in an exponential way (Hollis et al. 2019). The answer to that is beyond the scope of this paper, and we refer to (Cramwinckel et al., 2018; Hollis et al., 2019; O'Brien et al., 2017; Tierney et al., 2017) for detailed discussions, specifically about using TEX$_{86}$ in regions with SSTs warmer than modern. Following recent recommendations (Hollis et al. 2019), we here apply several calibrations to convert our TEX$_{86}$ values to SSTs. We apply an exponential calibration (Kim et al., 2010) for which we acknowledge that this calibration suffers from a regression dilution bias (Tierney and Tingley, 2015), and two linear calibrations; one on the warm part (>15°C) of the core-top dataset (O'Brien et al., 2017) and one using Bayesian statistics (BAYSPAR; Tierney and Tingley, 2015) to convert our TEX$_{86}$ values to SSTs. BAYSPAR produces a linear calibration based on a subset of the core top data with similar GDGT assemblages as the measured TEX$_{86}$, with a user-defined tolerance. The larger the subset of core tops (i.e., when the number of identified core-top analogues to the sample TEX$_{86}$ values is large), the closer the Bayesian calibration will approach a global linear regression. For MAAT reconstructions, we use the Deming regression of the soil-specific calibration of Naafs et al. (2017b; MAAT$_{soil}$) and the Bayesian BayMBT$_0$ of Dearing Crampton-Flood et al. (2020). The latter follows the approach of BAYSPAR, but then for MBT'$_{5me}$. We will compare the calibrations for both proxies to middle Eocene U$^{K'}_{37}$-based SSTs (from Bijl et al., 2010, but using BAYSPLINE calibration of Tierney and Tingley, 2018) and Paleocene–early Eocene sporomorph-based MAAT estimates (Contreras et al., 2014) from the same site.

Table 2. Calibration equations for TEX$_{86}$ and MAAT

Calibration	Equation	Type	Proxy for	Source
SST$_{exp}$ (TEX$_{86}^{H}$)	68.4 * log10(TEX$_{86}$) + 38.6	Exponential (regression dilution)	Mean annual SST (0–20m)	(Kim et al., 2010)

SST_{lin}	$58.8 * TEX_{86} - 11.18$	Linear	Mean annual SST (0–20m)	(O'Brien et al., 2017)
BAYSPAR	Prior mean = 20, prior std = 10, search tolerance = 0.15	Bayesian linear	Mean annual SST (0-20m)	(Tierney and Tingley, 2015)
$MAAT_{soil}$	$40.01 * MBT'_{5me} - 15.25$	Linear, Deming regression	Mean annual air temperature (for days above freezing)	(Naafs et al., 2017b)
$BayMBT_0$	Prior mean = 20, prior std = 15	Bayesian linear	Mean annual air temperature	(Dearing Crampton-Flood et al., 2020)

3.1.4 R-script for data analysis and evaluation

To facilitate systematic calculation of GDGT ratios, data analysis, visualization, and evaluation, we constructed a set of R markdowns (https://github.com/bijlpeter83/RGDGT.git) that can be applied to any time- or depth series of isoGDGT, brGDGT and/or brGMGT data. The R script loads peak areas of GDGTs/GMGTs from Microsoft excel spreadsheets, calculates and plots fractional abundances, overprinting indices and paleotemperature time or depth series.

3.2 Palynology

3.2.1 Sample processing

Palynological sample processing techniques were published in the original papers describing these datasets (Bijl et al., 2010; 2013b; Brinkhuis et al., 2003; Houben et al., 2019; Sluijs et al., 2011). We followed the same procedure for the new Maastrichtian–Paleocene samples. The different publications do indicate differences in the employed sieve mesh sizes (10 or 15 µm) but given all counted dinocysts are larger than 15 µm, this has not led to differences in the dinocyst results.

3.2.2 Taxonomy

We used the taxonomic framework cited in Williams et al., (2017) in our counts down to the species level, with one exception. For the Wetzelielloidae subfamily, we follow Bijl et al. (2017), for reasons stated therein. We also follow the supra-generic classification based on Fensome et al. (1993); genera described post-1993 were added into that classification accordingly.

3.2.3 Ecological affinities of dinocyst ecogroups

In this paper, we present our results plotted in eco-groups and complexes, which groups dinocyst species with similar ecologic affinities based on modern (for extant taxa) and empirical (for extant and extinct taxa) data (Frieling and Sluijs, 2018; Sluijs et al., 2005). The species of which the ecologic affinity was not assessed previously were included into larger groups based on shared morphological characteristics; primarily tabulation, archaeopyle and cyst- and process shapes. For example, the "*Apectodinium* complex" is equated to "Wetzellioids" following Frieling et al. (2014; see Table S2 for taxonomic grouping). We directly compare dinocyst- and terrestrial palynomorph indices with GDGT-based indices (following the approach of Frieling and Sluijs, 2018) to arrive at multi-proxy reconstructions of SST, river runoff and distance to shore (Table 3). For this, we resampled and binned GDGT-based indices to the sample resolution of the dinocyst data.

Table 3. Environmental parameters, and their corresponding GDGT indices and dinocyst eco-groups, based on Sluijs et al. (2005), Frieling and Sluijs (2018) and Sluijs and Brinkhuis (2009).

Environmental parameter	**GDGT index**	**Dinocyst eco-group**
Sea surface temperature	TEX_{86}	%Thermophiles (Wetzellioideae, *Hafniasphaera* spp., *Florentinia reichartii*, *Polysphaeridium* spp, *Homotryblium* spp., *Heteraulacacysta* spp., *Eocladopyxis* spp., *Dinopterygium* spp.)
Runoff, fresh water, salinity	IR, BIT	%*Senegalinium* cpx, %*Phthanoperidinium* spp., %Terrestrial palynomorphs
Distance to shore	BIT, #ringstetra	%Open marine (*Apectodinium* spp., *Impagidinium* spp., *Operculodinium* spp., *Spiniferites* spp.), %*Glaphyrocysta* cpx., %Epicystal Goniodomids (*Polysphaeridium* spp, *Homotryblium* spp., *Heteraulacacysta* spp., *Eocladopyxis* spp.,

		Dinopterygium spp.), %Terrestrial palynomorphs

3.2.4 Diversity and variability indices

To gain insight into the diversity and variability of the dinocyst assemblage through time, we employ several indices (Table 4), and compare their results at species and ecogroup level. We note that diversity in dinocyst taxonomy is complicated since dinocysts are dominantly produced during the hypnozygotic phase of the dinoflagellate life cycle following sexual reproduction. Only ~15% of modern dinoflagellates features this cyst stage (Fensome et al., 1993), which leaves a large proportion of the biological group unrepresented in the fossil record, including for example coral and foraminifer symbionts, but also more closely related free-swimming taxa. Dinocyst diversity can therefore only be used as an indicator for dinocyst-producing dinoflagellates. As a further complication, taxonomic divisions of cysts, although strongly related to dinoflagellate morphology and taxonomy, is fully based on the morphology of dinocysts. Even modern dinoflagellate-dinocyst relationships are often not unambiguous. Some dinoflagellate species produce various cyst morphologies (Rochon et al., 2008) that represent multiple cyst genera or species. Some of these cyst morphological variations are the result of ecology (Mertens et al., 2011). This complicates comparing cyst datasets on the species level and affects assessing biological diversity based on cysts. On the genus level, taxonomic division of cysts is in most cases based on plate tabulation, which is the morphologic feature that has the closest relationship to dinoflagellate biological diversity (Fensome et al., 1993). However, ecologic or biogeographic affinities have been established for some dinocysts on a species level (e.g., Frieling and Sluijs, 2018), which does suggest subtle morphological features may have biologic and ecologic significance. The eco-groups we use here are the result of extensive reviews of empirical data. These groups combine dinocyst genera and species with fundamentally similar plate tabulations, and thus probably group cysts of closely affiliated biological dinoflagellate species, and, as such also ecologic affinities. For our diversity calculations we use both the ungrouped data on species level and the diversity in dinocyst ecogroups.

As the simplest approximation of biological diversity, the richness R in terms of dinocyst taxa was summed. Furthermore, several diversity measures were calculated using the R package Vegan (Oksanen et al., 2015). Of these, Fisher's alpha (α) is based on the count data, whereas the Shannon index (H') and Simpson index (D) derive from the relative abundance data. Finally, we employed the Σcv metric (Gibbs et al., 2012), which we here dub the "Gibbs index", and which provides a measure for assemblage variability. Together, these metrics can give insight into changing stability and diversity of these regional dinocyst assemblages over the Maastrichtian to early Oligocene.

Table 4. Diversity and variability indices for (fossil) assemblages. In the Shannon and Simpson indices, p_i represents the proportional abundance of the i^{th} taxon of the total amount of taxa R. The Gibbs index summates the coefficients of variation (SD/mean) of all taxa (i to R) over a certain rolling window $t_1 \rightarrow t_2$. In Fisher's alpha, the α parameter is estimated from the dataset in which S is the expected number of species with an abundance of n. x represents a nuisance parameter estimated from the dataset, generally between 0.9 and 1. While the Gibbs index is calculated over a rolling window, the other indices are calculated per sample.

Index	**Equation**	**Source**
Shannon index (H')	$H' = \sum_{i=1}^{R} p_i * \ln p_i$	(Shannon, 1948)
Simpson index (D)	$D = \sum_{i=1}^{R} p_i^2$	(Simpson, 1949)
Gibbs index (Σcv)	$\Sigma\mathrm{cv} = \sum_{i=1}^{R} \left(\frac{\mathrm{SD}_{i,t_1 \rightarrow t_2}}{\mathrm{mean}_{i,t_1 \rightarrow t_2}} \right)$	(Gibbs et al., 2012)
Fisher's alpha (α)	$S_n = \frac{\alpha x^n}{n}$	(Fisher et al., 1943)

3.3 Comparison of GDGT and dinocyst assemblage data

https://doi.org/10.5194/cp-2021-18
Preprint. Discussion started: 11 March 2021

Both dinocyst ecogroups and GDGT indices bear information on SST, runoff (~salinity), nutrients and marine primary productivity, and relative distance to shore (Table 4). As dinocyst and GDGT analyses were performed on partly separate datasets, the highest resolution dataset (dinocysts) was linearly resampled to the depth intervals of the GDGT data to facilitate inter-comparison.

4. Results

4.1 GDGTs

The resulting dataset has an average temporal resolution of ~130 kyrs for the time interval between 70 and 30 Ma. IsoGDGTs dominate the pool of GDGTs (particularly GDGT-0 and crenarchaeol), with a gradual increasing relative abundance of brGDGTs (particularly Ia) throughout the record (Fig. 3). BrGMGTs are in low (<10%) relative abundance, except in the Oligocene, where they account for up to 30% of the total GDGT/GMGT pool.

4.1.1 Isoprenoidal GDGTs

Before the TEX_{86} index results (Fig. 4a) can be interpreted in terms of SST, we assess whether the isoGDGTs are primarily derived from the sea surface, or have received contributions from non-pelagic sources. Across the Ypresian, the BIT index (Fig. 4b) increases from values around 0.1 in the underlying sediments to values at times exceeding 0.4. Most EECO and middle Eocene values, however, have BIT index values between 0.2 and 0.35. The remaining sediments have BIT index values of around 0.3, with the exception of some upper Eocene and Oligocene sediments that occasionally have values around 0.75. There is no correlation between TEX_{86} and BIT in our entire dataset (p=0.15). None of the samples have fcren' (Fig. 4c) values above the cut-off of 0.25, suggesting no non-temperature related contribution of the crenachaeol isomer to the isoGDGTs. In fact, the consistent trend in (fcren') and the TEX_{86} index (Fig. 4) (and TEX_{86}^{L}, not shown) demonstrates the temperature sensitivity of cren' and confirms that discarding it from the index as was done for the cold-temperature index TEX_{86}^{L} (Kim et al., 2010) is not justified here. With the exception of 6 samples in the Oligocene, all samples have methane index values below the conservative cut-off value of 0.3 (Fig. 4d), although in the early and middle

Eocene, methane index values do approach the cut-off. AOM ratio values suggest an overprint from anaerobic methane oxidisers in one sample in the early Eocene that also has a high BIT index, and 5 samples from the Oligocene where isoGDGTs supposedly received a contribution of anaerobic methane oxidisers (Fig. 4e). As a result, these samples were discarded for TEX_{86}.

Fig. 4

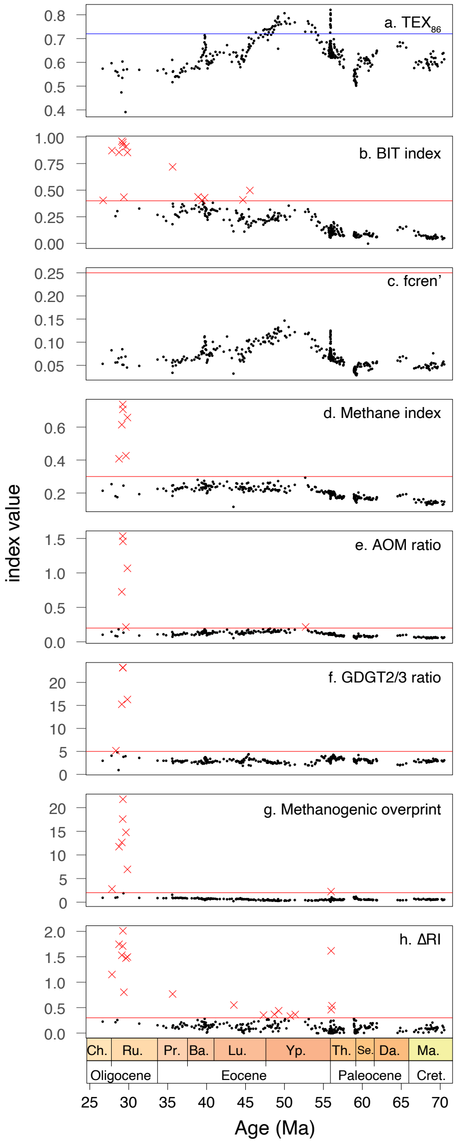

Figure 4. TEX_{86} index and overprinting indices. For the equations of these indices see Table 1. Red line indicates the cut-off value, red crosses indicate samples exceed the cutoff a. TEX_{86} (Schouten et al., 2002), with blue line indicating the maximum modern core-top value (~0.72). b. BIT index (Hopmans et al., 2004). c. fcren' (O'Brien et al., 2017), no samples discarded; d. Methane index (Zhang et al., 2011), $n_{discarded}$ = 6. e. AOM ratio (Weijers et al., 2011), $n_{discarded}$ = 6. f. GDGT2/3 (Taylor et al., 2013), conservative cut-off of 5, $n_{discarded}$ = 4, one sample retained for absence of anomalous Ring index values (see text). g. Methanogenesis (Blaga et al., 2009), cut-off of 2.0, $n_{discarded}$ = 8. h. ΔRI $n_{discarded}$ = 18.

Values signalling a deeper water column overprint (GDGT2/3 ratio) fall below 5 for most of the data (Fig. 4f), which was expected given the depositional setting on a continental shelf. A total of 5 samples has water GDGT2/3 values exceeding 5, 4 of which also had other indications of overprinted isoGDGT signals. We discard eight TEX_{86} datapoints because GDGT-0/crenarchaeol ratios are over 2 (Fig. 4g). One of these is from the PETM, with a value just above the cut-off. The others represent Oligocene samples.

In total, 18 samples fall outside the range of RI values that characterize modern pelagic-derived isoGDGT compositions (ΔRI >0.3; Fig. 4h, or 95% confidence interval; Fig. 5). Nine of these 18 come from the interval >43 Ma and have no other indications of overprints. These samples fall just outside the 95% confidence interval limits (Fig. 5) and do follow the overall RI/TEX_{86} trend, but we here discard them to be conservative. The other 9 samples with too high ΔRI come from the late Eocene-Oligocene and have BIT index values over 0.4. Two of these samples have no other overprint indication, the other 7 have multiple other overprints. One sample has RI values above the range of modern samples (with no other overprinting indications), the others have too low RI values. Eight samples with normal RI values do have overprints based on the other indices: BIT index values slightly over 0.4 (6 samples), GDGT2/3 ratio values over 5 (1 sample), and AOM ratio over 0.2 (1 sample). Following Leutert et al. (2020) we retained the samples with normal RI values and

https://doi.org/10.5194/cp-2021-18
Preprint. Discussion started: 11 March 2021

high BIT or GDGT2/3 ratio values. After considering all these potential biases, and retaining those with normal isoGDGT distributions, we discard a total of 19 samples. Most discarded samples are from the Oligocene and meet multiple overprint criteria.

Fig.5

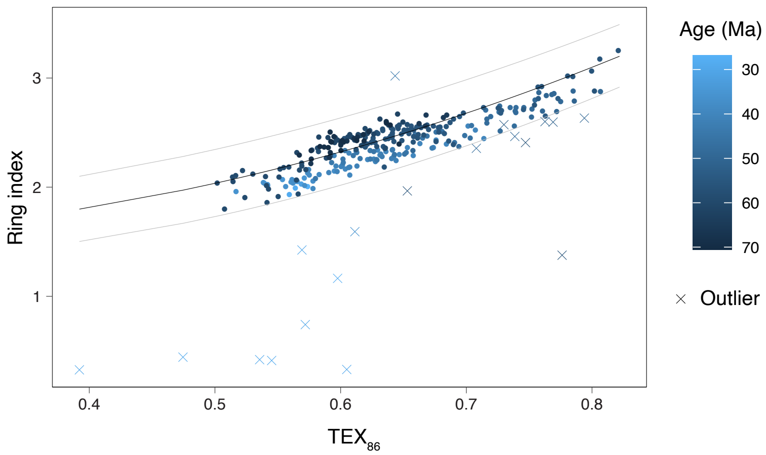

Figure 5. Ring index (RI) versus TEX$_{86}$. Dots indicate RI/TEX$_{86}$ values for samples that are retained, crosses indicate samples that are discarded (see Fig. 4). Color of all datapoints indicates age of the sample, from Maastrichtian (dark blue) to Oligocene (light blue). Black and grey curves represent the RI/TEX$_{86}$ relationship of modern core top samples, and 95% confidence interval, respectively.

4.1.2 Branched GDGTs

Before brGDGT distributions can be interpreted in terms of air temperature, we assess whether they are primarily derived from soils, or have received contributions from river-, or marine in situ production. The relative abundance of tetra-, penta- and hexamethylated brGDGTs in the samples from 1172 deviates from that in modern and Paleogene soils and peats (Fig. 6): it has either comparatively less tetra-, less penta-, or more hexamethylated brGDGTs, and the data split into 2 clusters. The largest cluster follows the distribution observed in modern soils and peats with an offset (Fig. 6). This generally indicates brGDGT contributions from sources other than soils. The smaller second cluster, containing exclusively mid-to-late Paleocene samples, is indeed close to that of modern continental shelf sediments

(Svalbard and Berau delta; Dearing Crampton-Flood et al., 2019; Sinninghe Damsté, 2016) for which in situ brGDGT production substantially exceeds soil contributions. This would generally suggest that the smaller cluster, and perhaps also the larger cluster of samples, have contributions from marine in-situ brGDGT production. However, unlike those modern marine sediments, our entire record does not show elevated #rings$_{tetra}$ values that are associated to marine *in situ*-produced brGDGTs (Fig. 7). The low #rings$_{tetra}$ values on our record (<0.3) suggest brGDGTs have a terrestrial source.

Fig. 6

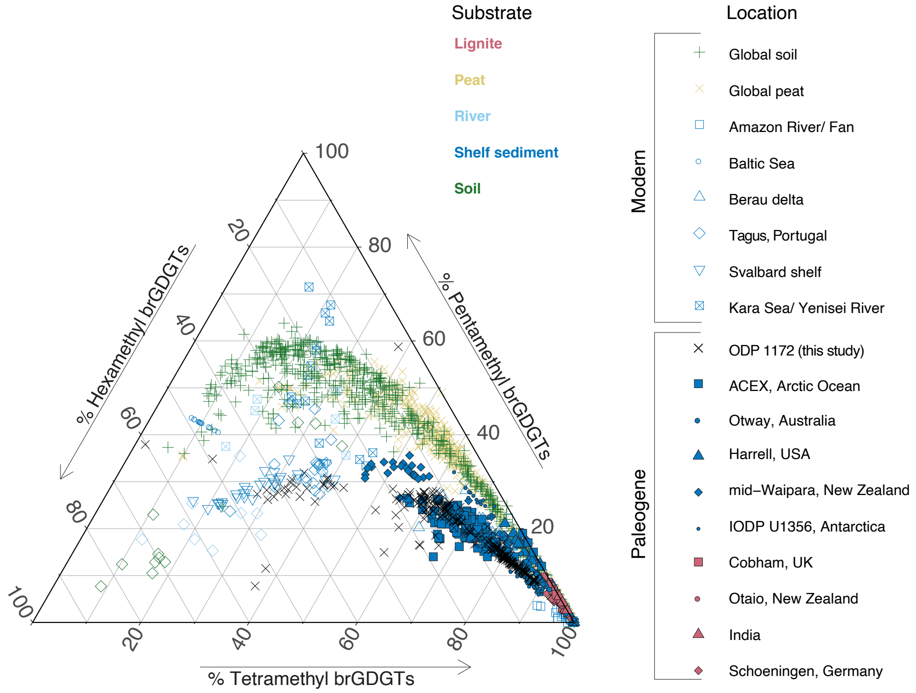

Figure 6. Ternary diagram showing fractional abundance of tetra-, penta- and hexamethylated brGDGTs from modern soils (Dearing Crampton-Flood et al., 2020), peats (Naafs et al., 2017b), rivers (Tagus River, Portugal (Warden et al., 2016) and Yenisei River (De Jonge et al., 2015)) and marine sediments (Kara Sea (De Jonge et al., 2015), Svalbard (Dearing Crampton-Flood et al., 2019), Berau delta (Sinninghe Damsté, 2016), Portugal (Warden et al., 2016), Baltic Sea (Warden et al., 2018), and

Amazon Fan (Zell et al., 2014)), Paleogene lignites (Cobham, Schoeningen, India and Otaio (Naafs et al., 2018b)) and Paleogene marine sediments (Arctic Ocean, IODP Arctic Coring Expedition ACEX (Willard et al., 2019), Otway Basin, Australia (Huurdeman et al., 2020), Gulf of Mexico coastal plain, Harrel core (Sluijs et al., 2014), New Zealand (Pancost et al., 2013) and Antarctic Margin IODP Site U1356 (Bijl et al., 2013a)). Data from ODP Site 1172 in black crosses.

Fig.7

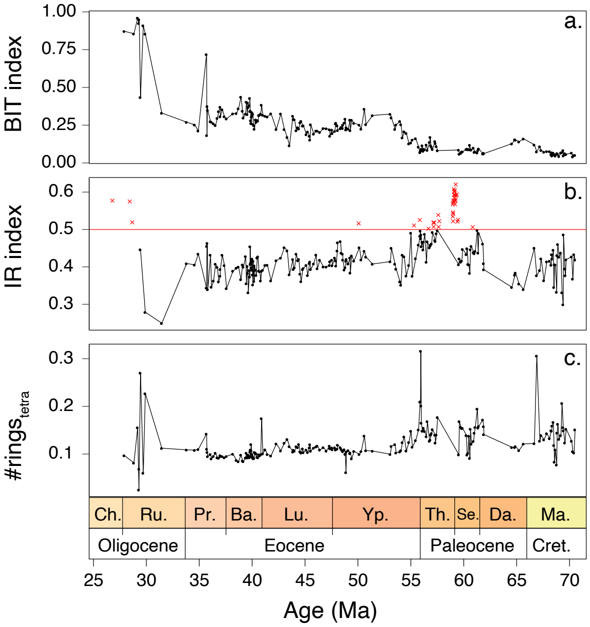

Figure 7. a. BIT index, b. IR (with cut-off value of the Australian soil IR of 0.5 and discarded MAAT samples in red crosses) and c. #rings$_{tetra}$ from Site 1172.

In the modern soil- and peat brGDGT dataset #rings$_{penta}$ and #rings$_{tetra}$ are below 0.7 and follow a coherent 1:1 correlation (Fig. 8a). Values >0.7 suggest brGDGTs cannot come purely from soils (Sinninghe Damsté 2016). All samples from 1172 are below 0.7 for both these indices, which suggests a terrestrial origin is likely, and a strong contribution by marine in situ produced brGDGT is unlikely. We do note that while #rings$_{tetra}$ is below 0.3, #rings$_{penta}$ ranges up to 0.6. This diverts from the

1:1 line but brings the brGDGT dataset from Site 1172 within the area of other Paleogene marine brGDGT datasets (Fig. 8a). This is consistent with the relative abundances of tetra-, penta- and hexamethylated brGDGTs plotted in the ternary diagram, where all Paleogene data plotted offset to that in modern soils. #rings$_{tetra}$ and #rings$_{penta}$ for the 5- (Fig. 8b) and 6-methyl brGDGTs (Fig. 8c) separately shows that the diversion of the 1172 data from modern soils and peats is primarily caused by a larger degree of cyclisation of the 6-methyl brGDGTs, suggesting an influence by river brGDGT production.

The samples within the Paleocene cluster do have relatively high IR. The IR in our record averages ~0.4, but is elevated between 62 Ma and 54 Ma, with peak values in the mid-Paleocene up to 0.6 (Fig. 7). Although based on only two datapoints, modern southeast Australian soils have IR values of maximum 0.5 (De Jonge et al., 2014a). Hence, any values exceeding that of the corresponding hinterland soils could indicate a contribution by non-soil sources (be it marine or river in situ production; De Jonge et al., 2014a). Given that #rings indices values argue against a large contribution from marine in-situ production, we suggest that river-produced brGDGTs contribute to the GDGT pool in the Paleocene samples with high IR. Therefore, for MBT'$_{5me}$ calculation, we eliminate all brGDGT samples in our record that have IR values above that of Australian soils. The IR$_{penta}$ and IR$_{hexa}$ are well within the range of the modern soil and peat data (Fig. 8d) and settings affected by marine or river in situ production (Svalbard, Kara / Yenisei), and plot far away from lignite deposits.

Fig.8

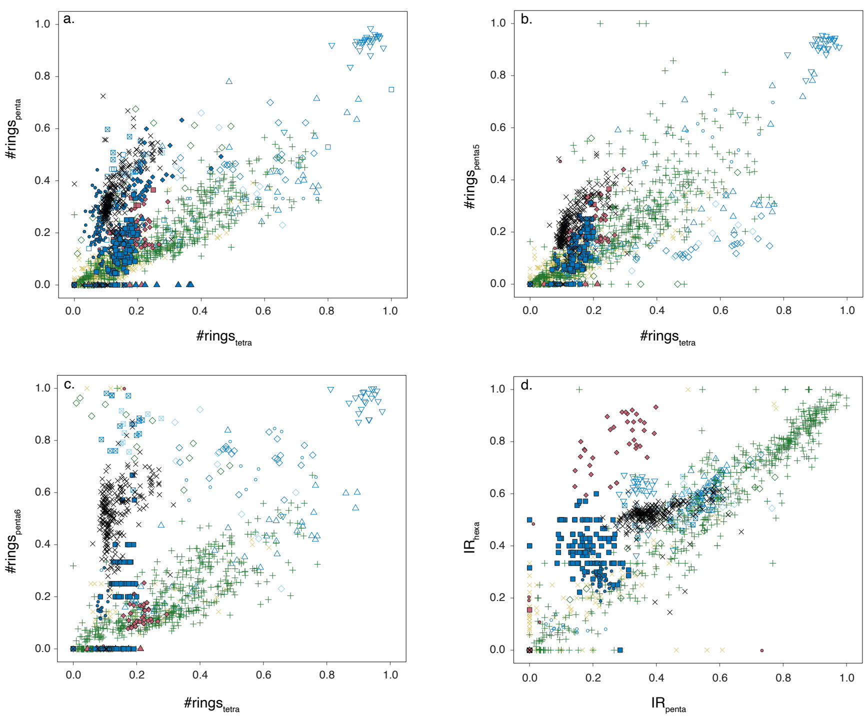

Figure 8. Crossplots of various brGDGT indices. a. #rings$_{tetra}$ *vs.* #rings$_{penta}$, #rings$_{tetra}$ *vs.* #rings$_{penta5}$, #rings$_{tetra}$ *vs.* #rings$_{penta6}$, IR$_{penta}$ *vs.* IR$_{hexa}$. For color and symbol legend see Figure 6.

The consistent offset in brGDGT composition in Paleogene marine sediments relative to modern soils can potentially be explained by non-soil contributions even though many (most) indices suggest soil-dominated sourcing. Notably, not only Paleogene marine sediments from Site 1172 are offset from present-day soils, but this extends to other sites as well, including Paleogene lignites that are not influenced by marine contributions. We thus argue that there may be an additional evolutionary- or bacterial community factor that is at least in part responsible for the observed offset brGDGT distributions during the Paleogene, and argue that, with some exceptions where indices do suggest non-soil contributions, Paleogene marine sediments contain a dominant soil-derived brGDGT signal in spite of their offset composition.

4.2 SST and MAAT reconstructions

4.2.1 SST

By removing all samples with potential overprint from the record we can now assess the trends in TEX_{86}-based SST (Fig. 9a). Reconstructed SSTs differ to up to 4 °C between the exponential SST_{exp} and the linear SST_{lin} calibration in the warmest intervals, and progressively less with lower SSTs (Fig. 9a). The BAYSPAR method, which uses a linear relation between SST and TEX86 generates the lowest SSTs for the low TEX_{86} values in the Maastrichtian, Paleocene and middle–late Eocene, and SSTs in between those based on the linear and exponential calibrations for the highest TEX_{86} index values (Fig. 9a). $U^{K'}{}_{37}$-based SSTs (Bijl et al., 2010, with BAYSPLINE calibration) around the MECO are most consistent with the high SSTs based on the linear TEX_{OBL} calibration, although in this TEX_{86} range all calibrations yield SSTs within error (Fig. 9a).

In general, Maastrichtian (70.5–66.7 Ma) SSTs show a gradual cooling trend towards the late Maastrichtian–early Danian hiatus of ~800 kyrs. The early Danian (~65 Ma) is roughly 3 °C warmer than the late Maastrichtian (~67 Ma). The mid-Paleocene (62–59 Ma) shows two cooling steps: a ~2 °C cooling at 62 Ma, followed by a return to higher SSTs roughly at 60 Ma, and a ~5 °C cooling to minimum values of around 18°C around 59.5 Ma, where the record is truncated by a hiatus.

A hiatus straddling the early Thanetian (59.0–57.7 Ma) likely obscures the onset of late Paleocene warming out of the mid-Paleocene temperature minimum. Background latest Paleocene SSTs fluctuate considerably, but the PETM warming clearly stands out (Sluijs et al., 2011), with a magnitude (5-7 °C depending on the calibration) comparable to that in other mid- to high latitude sections and similar to the global average (Frieling et al., 2017). Post-PETM SSTs drop back to pre-PETM values completely, followed by renewed warming towards the EECO. The magnitude of warming is 6 to 11 °C depending on the choice of calibration. Smaller early Eocene hyperthermal events, if represented in our record, do not clearly stand out at Site 1172.

Highest SSTs of the EECO are slightly lower than peak PETM values in all calibrations, consistent with other records (Inglis et al., 2020). However, a hiatus between 52.7 and 51.4 Ma may conceal peak EECO temperatures (Hollis et al., 2019; Lauretano et al., 2018). A gradual SST decline commences around 49.2 Ma and terminates the EECO, which is broadly coeval with cooling inferred from benthic foraminiferal isotope records (Lauretano et al., 2018) and proxy records from New Zealand (Dallanave et al., 2016; Crouch et al., 2020).

Fig.9

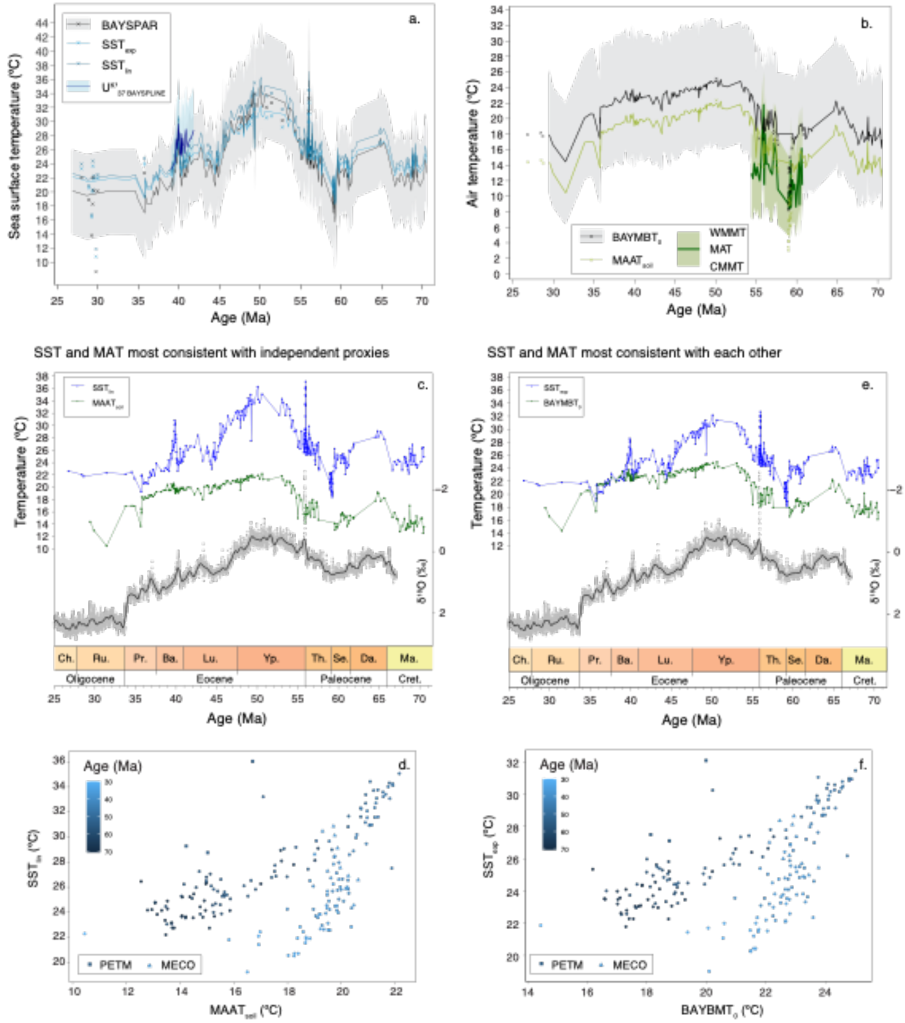

Figure 9. Paleothermometers. a. TEX$_{86}$ based SST reconstructions, using a Bayesian (BAYSPAR; black, with 90% confidence interval in grey envelope; Tierney and

Tingley, 2015) an exponential (SST_{exp}; light blue; Kim et al., 2010) and a linear (SST_{lin}; dark blue; O'Brien et al., 2017) calibration. Also plotted are $U^{K'}_{37}$ -based SSTs (thick blue line; from Bijl et al., 2010, recalculated using BAYSPLINE of Tierney and Tingley, 2018). Discarded samples are indicated by the crosses. b. brGDGT-based MAAT reconstructions using the Bayesian ($BayMBT_0$; black, with 90% confidence interval in grey envelope; Dearing Crampton-Flood et al., 2020) and soil ($MAAT_{soil}$; light green; Naafs et al., 2017b) calibrations. Discarded samples are indicated in crosses. Also plotted are pollen-based NLR-approach MAT reconstructions (thick dark green, with light green envelope representing coldest and warmest month mean temperatures; from Contreras et al., 2014). c. SST and MAAT reconstructions using the calibrations that are most consistent with independent proxies from this site (Bijl et al., 2010; Contreras et al., 2014), with the CENOGRID benthic foraminifer oxygen isotope splice of Westerhold et al., 2020 (10pnt loess smooth in grey, 500 pnt loess smooth in black). d. cross-correlation between SST_{lin} and $MAAT_{soil}$. e. SST and MAAT reconstructions using the calibrations that are, in absolute temperature, most consistent with each other, with the CENOGRID benthic foraminifer oxygen isotope splice of Westerhold et al., 2020 (10pnt loess smooth in grey, 500 pnt loess smooth in black). f. cross-correlation between SST_{exp} and $BAYMBT_0$.

Post-EECO cooling is gradual and of small magnitude (2 °C from peak EECO values) until about 46.4 Ma, after which it accelerates (5 °C) between 46.2 Ma and 44.4 Ma. The age model in this particular part of the sequence is complicated, due to a problematic assignment of chron C21n (Bijl et al., 2010; 2013b). Following the minimum SSTS at 44.4 Ma, SSTs rise again towards a plateau at 42.7 Ma. An SST minimum of ~22 °C is observed just prior to the MECO, at 40.2 Ma, followed by MECO warming of about 5–7 °C reached at 39.9 Ma. Post-MECO cooling seems more gradual than MECO warming, although this might be the result of sedimentation rate changes (Bijl et al., 2010), which are not accounted for in our age model. SSTs are almost identical to those for the MECO at nearby Site 1170 on the South Tasman Rise (Cramwinckel et al., 2020). Post-MECO cooling transitions into gradual late Eocene cooling, down to a minimum of ~19 °C at 35.7 Ma. The following latest Eocene to

Oligocene TEX_{86}-based SSTs (35–27 Ma) are 3 °C warmer, with surprisingly no cooling associated to the Eocene–Oligocene transition (Houben et al., 2019).

4.2.2 MAAT

After excluding samples with IR values above those of local soils, we present MBT'_{5me}-based MAAT reconstructions. These differ substantially (up to 5°C) per calibration chosen (Fig. 9b). The $MAAT_{soil}$ calibration yield consistently cooler MAATs (2–3°C) compared to the $BAYMBT_0$ calibration (Fig. 9b), which may be because the $MAAT_{soil}$ is calibrated against average temperature of the days above freezing, while $BAYMBT_0$ is calibrated against mean annual temperature. Both MAAT calibrations fall between the MAT and the warmest month mean temperature reconstruction of the sporomorph nearest living relative (NLR)-based temperature reconstruction (Contreras et al., 2014), and calibration errors largely overlap.

Independent of the calibration chosen, MAAT evolution reveals late Maastrichtian-early Danian warming of 3°C, gradual 4°C cooling towards the mid-Paleocene, gradual 8°C warming towards the EECO, with a conspicuous absence of warming at the PETM. Gradual cooling of 4°C starts at 49.5 Ma and continues into the Late Eocene. MAAT reaches a minimum at 43 Ma, followed by a plateau-phase. There is little warming that can be associated to the MECO. MAAT shows a conspicuous transient 3 °C cooling in the Late Eocene, at the onset of glauconite deposition. The Eocene-Oligocene Transition is characterized by another 5°C MAAT cooling.

Fig. 10

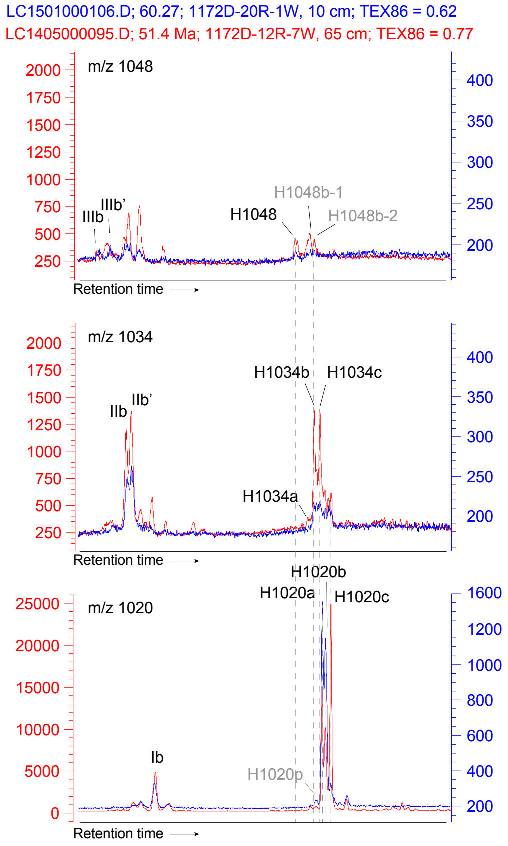

Figure 10. Stack of 2 UHPLC-MS chromatograms (1172D-12R-7W, 65cm in red and 1172D-20R-1W, 10cm in blue) of *m/z* 1048, 1034 and 1020 traces, between ~40 and ~60 minutes retention time, showing the pattern of peaks corresponding to brGDGTs and brGMGTs. Peak labels refer to the molecular structures in Fig. 3.

4.3 brGMGTs

We detected brGMGTs throughout the record (see Fig. 10 for typical chromatograms). The exact molecular structure and position of the C-C bridge is still unknown but based on visual comparison with chromatograms of brGMGTs in African lake sediments (Baxter et al., 2019), all 7 known brGMGTs can be identified.

Next to H1020a, b, and c as most abundant brGMGTs, also H1034a, b and c are detected, although in some samples in the Maastrichtian, individual peaks could not be separated. Traces of H1048 can be seen at times, suggesting presence of this compound as well, albeit in low relative abundance. Next to these previously described peaks, we here recognized several other peaks that consistently occur at Site 1172: one compound that elutes just prior to H1020a, which we term H1020p (Fig. 10). ~1 minute after H1048 elutes, two more peaks appear which we here term H1048b-1 and H1048b-2 (Fig. 10). Because these have so far unknown affinities or molecular structure, we do not include them here further in our calculations.

Fig. 11

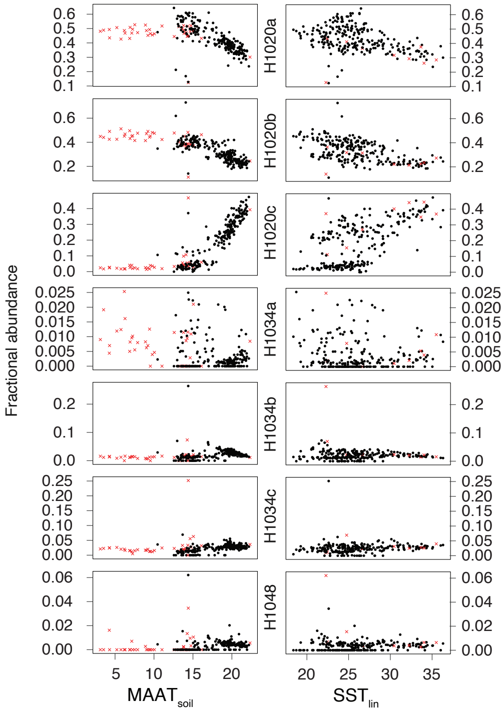

Figure 11. Fractional abundances of brGMGTs plotted against BAYMBT$_0$ and SST$_{exp}$.

The fractional abundances of the H1020 isomers show qualitatively similar relations to temperature as in the East African lake dataset of Baxter et al. (2019): H1020b abundance has a negative relationship with MAAT, while H1020c has a

https://doi.org/10.5194/cp-2021-18
Preprint. Discussion started: 11 March 2021

positive relationship (Fig. 11). In addition, H1020a seems negatively correlated with MAAT in our data, although this compound does not show any relation to temperature in lakes (Baxter et al., 2019). The relative abundances of the H1034 isomers do not show a clear relationship with MAAT (Fig. 11), similar as in the tropical lake dataset, where the scatter increases at lower (H1034b) or higher (H1034a, c) temperatures (Baxter et al., 2019).

Downcore trends in brGMGTI are primarily controlled by the relative abundance of H1020c and closely follow those in both SST and MAAT. Upon cross-correlation, we note that brGMGTI has a higher correlation with MAAT (R = 0.89) than with SST (R=0.57; Fig. 12). Interestingly, the correlations between brGMGTI and temperature indices only hold for part of the dataset. Samples with high IR values, for which brGDGT-based MAAT could not be reliably interpreted, fall outside the correlation (grey crosses in Fig. 12). This is probably due to the supposed contribution of river-derived brGDGTs that may bias MAAT towards lower temperatures. In addition, we also note that brGMGTI approaches 'saturation' (brGMGTI = 0) at reconstructed MAAT of 15°C. The correlation with temperature (MAAT and SST) is divided into 2 clusters. BrGMGTI values for samples from the younger part of the record, with BIT index <~0.3, seem to correlate better to temperature than those from the older part of tha record, with BIT index values >~0.3 (Fig. 12). In the Oligocene, where many isoGDGT signals were evidently overprinted, the %brGMGTs increases (Fig. 3, 12d), and the brGMGT composition is characterized by a relatively higher abundance of H1020c, H1034b and H1048 compared to the rest of the record (Fig. 3; 12).

There is no clear relationship between %brGMGTs and MBT'$_{5me}$-based MAAT (Fig. 12h, i). This slightly differs from the Paleocene-Eocene Arctic Ocean record (Sluijs et al., 2020), where the brGMGTI has no correlation to temperature, while %brGMGTs do. This may indicate differences in sources of brGMGTs between the sites, differences in oceanographic settings, or a non-temperature control on their distribution. HMBT$_{acyclic}$ does seem to show similar trends to the MBT'$_{5me}$-based MAAT (Fig. 12g), like in the Arctic Ocean (Sluijs et al., 2020).

Fig. 12

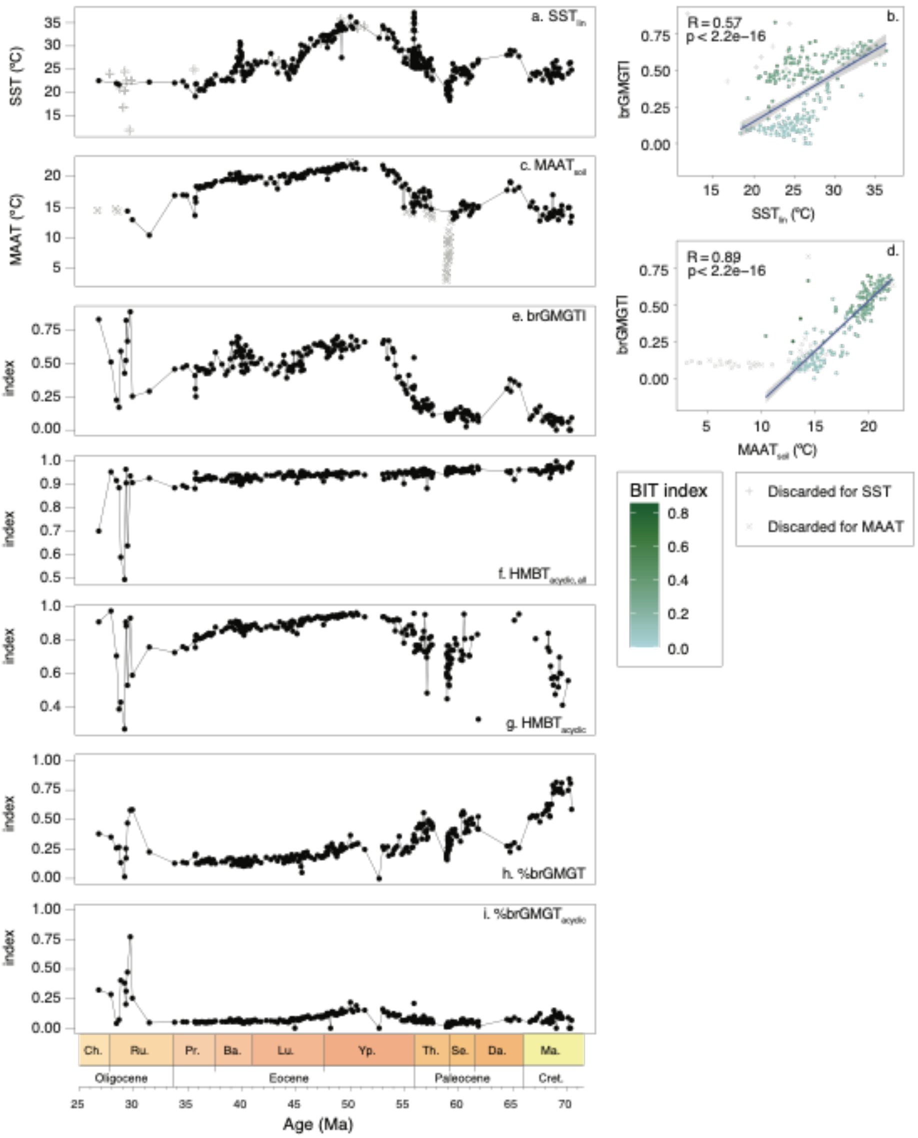

Figure 12. Time series and crossplots of brGMGT-based indices with MAAT and SST reconstructions. (a) $\mathrm{SST}_{\mathrm{lin}}$ (b) crossplot of $\mathrm{SST}_{\mathrm{lin}}$ and brGMGTI, (c) $\mathrm{MAAT}_{\mathrm{soil}}$, (d) crossplot of $\mathrm{MAAT}_{\mathrm{soil}}$ and brGMGTI, (e) brGMGTI, (f) $\mathrm{HMBT}_{\mathrm{acyclic,\ all}}$, (g) $\mathrm{HMBT}_{\mathrm{acyclic}}$, (h) %brGMGT (Baxter et al., 2019), (i) $\%\mathrm{brGMGT}_{\mathrm{acyclic}}$ (Naafs et al., 2018). For equations see Table 1). Colour variable in the crossplots indicate the BIT index value.

4.4 Palynology

4.4.1 Assemblages

Dinocyst assemblages are dominated by *Manumiella* spp. throughout the Maastrichtian, together with Goniodomideae (notably *Dinopterygium* spp.), and *Cerebrocysta* cpx. (Fig. 13). From the late Maastrichtian onwards, *Senegalinium* cpx. increases gradually in relative abundance, interrupted by acmes of *Palaeoperidinium pyrophorum* in the Danian and *Glaphyrocysta* cpx. in the lower Selandian. Relative abundances of *Senegalinium* cpx. reach maximum values during the mid-Paleocene and during the Paleocene–Eocene transition, while the PETM itself is characterised by abundant *Apectodinium* (~30%) and common *Senegalinium* cpx. and Goniodomideae (Sluijs et al., 2011). After the PETM, *Senegalinium* cpx. abundances temporarily increase, and are then replaced by *Deflandrea* cpx, *Spinidinium* cpx and *Elytrocysta* spp. and low abundances of various other genera, e.g., *Wetzeliella*, *Hystrichokolpoma*, Goniodomideae (Fig. 13). From 45 Ma to ~37 Ma, *Enneadocysta* spp. alternates dominance with *Deflandrea* cpx. and *Spinidinium*/*Vozzhennikovia* cpx, with contributions of *Phthanoperidinium* spp. (Röhl et al., 2004a). Protoperidinioid dinocysts appear commonly in the late Eocene, around 35.5 Ma (Houben et al., 2019; Sluijs et al., 2003; Fig. 13).

4.4.2 Diversity and variability

Together with the changing assemblage composition are some strong and coherent changes in all diversity and variability indices (Fig. 14). First, results are highly similar for the full species-level dataset and the grouped assemblages, indicating robustness of both the grouping and diversity analysis. The Maastrichtian–Paleocene assemblages are characterized by relatively low diversity, which increases towards the EECO, as variability indicated by the Gibbs index decreases. After this, diversity drops and variability increases during middle–late Eocene cooling ~49–38 Ma, with an interruption around 41–39 Ma. Towards the top of the record, both diversity and variability increase.

https://doi.org/10.5194/cp-2021-18
Preprint. Discussion started: 11 March 2021

Fig. 13

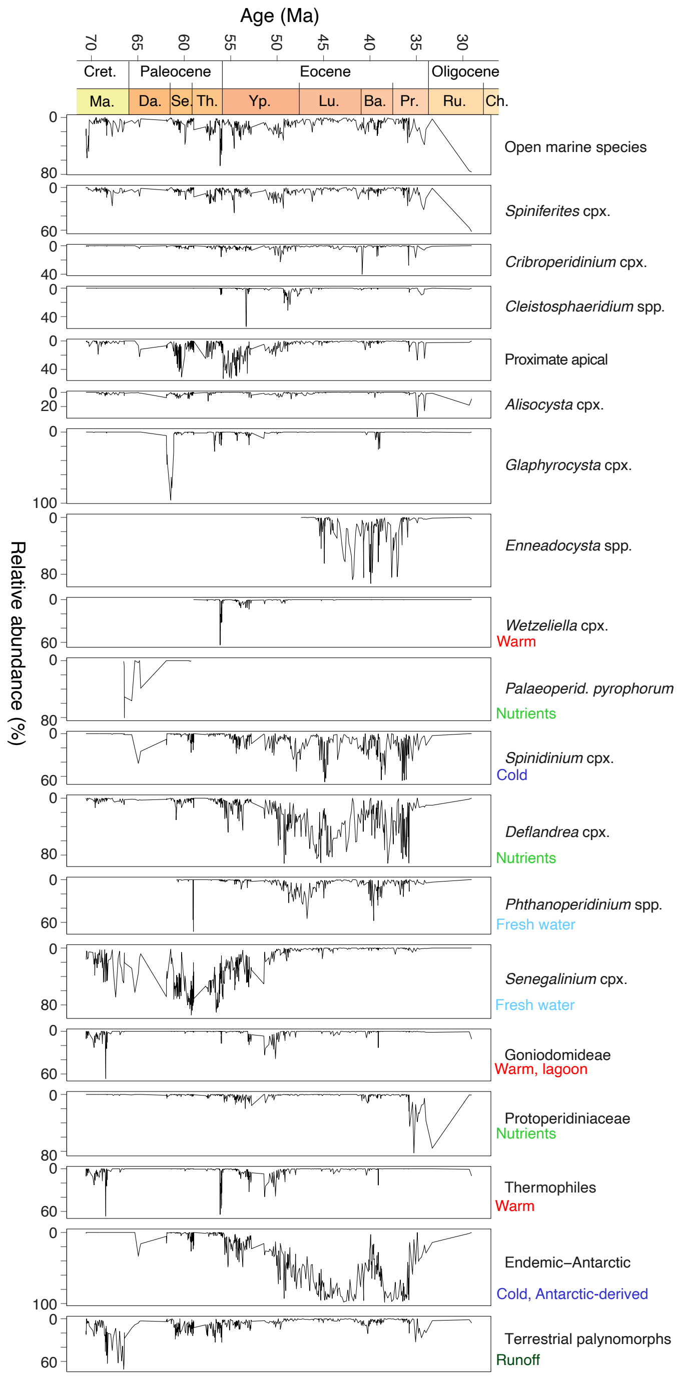

https://doi.org/10.5194/cp-2021-18
Preprint. Discussion started: 11 March 2021

Figure 13. Dinocyst ecogroups and %terrestrial palynomorphs from Site 1172. From left to right, ecogroups are ordered in an in-shore-to-offshore transect. Relative abundance ticks represent 20%.

Fig. 14

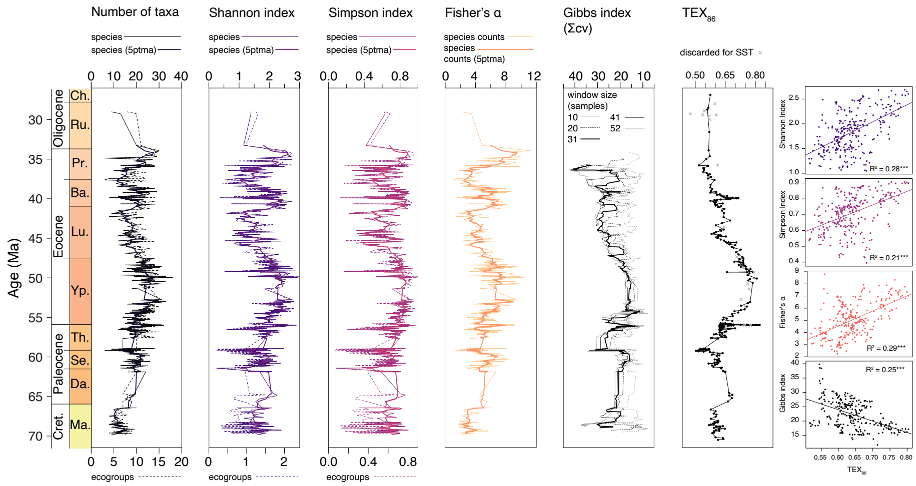

Figure 14. Dinocyst taxonomic diversity and variability through time. From left to right are plotted number of taxa (black), Shannon index (purple), Simpson index (pink), Fisher's alpha (orange) (species-based dataset in solid lines; ecogrouped dataset in dashed lines) and Gibbs index (different window sizes in gray-black). TEX_{86} plotted for comparison. Crossplots show correlation of these indices with TEX_{86}.

5. Discussion

5.1 Air and sea surface temperature evolution compared

The near-shore depositional setting of our record should have captured a coastal terrestrial environment with similar MAATs similar to the local SSTs. Indeed, the brGDGT-based MAAT record shows strong similarities to SST particularly in multi-million year trends (Fig. 9). Specifically, the early Danian is warmer than the Maastrichtian, and bothe records show a 2-step Paleocene cooling, late Paleocene warming towards peak values in the EECO, and middle–late Eocene cooling. On shorter time scales both records, occasionally even on sample-to-sample level, show synchronous variability (Fig. 9c, d). The independent SST (based on alkenones; Bijl et al., 2010) and air temperature reconstructions (based on pollen assemblages; Contreras et al., 2014) show the best fit with the absolute SST values derived from the linear calibration for TEX_{86} (BAYSPAR or SST_{lin}; generating the highest SST estimates), and MAATs based on the calibration using Deeming regression ($MAAT_{soil}$), respectively. These are the two calibrations with the largest absolute temperature offset, particularly in the warm EECO (Fig. 9c). If the local terrestrial climate in the nearby river catchment is largely controlled by ocean temperature, the absolute mean annual SST and MAAT should be broadly similar in the integrated signal of our samples. This could be an argument to choose transfer functions for SST and MAAT whereby absolute temperature estimates overlap most: SST_{exp} and the Bayesian $BAYMBT_0$. These generate overlapping absolute temperatures for the colder middle-late Eocene and Paleocene, but in the warmer Eocene time intervals SSTs remain consistently warmer (by ~8 °C). The lower MAATs cannot be explained by a saturation of the MBT'_{5me} index that is underlying the paleothermometer, as maximum recorded MBT'_{5me} values are around 0.85 in the EECO. Accounting for the calibration errors of SST (±2.5 °C) and the large calibration error bar of $BAYMBT_0$ in principle could resolve the offset but applying the extremes in calibration error to TEX_{86} and MBT'_{5me} to make them consistent would make both profoundly inconsistent to the other independent SST and MAAT proxies from the same samples. More importantly, the colder MAAT compared to SST seems to be a consistent feature in many regions where TEX_{86} and MBT'_{5me} were applied together (see e.g., Hollis et al., 2019 and compare Willard et al., 2019 and Sluijs et al., 2020). The offset between MAAT and SST would have been more variable between sites if it were only the result of calibration errors. TEX_{86} -based SSTs in the southwest Pacific realm have been on the high end of many multi-proxy-based temperature reconstructions for the Eocene (Hollis et al., 2012), and therefore may be assumed to have an as yet poorly understood warm bias. However, the consistency of TEX_{86}-based SSTs with other SST proxies for specific time intervals and locations (Bijl et al., 2010; Hines et al., 2017) suggests the SST-MAAT offset cannot be easily reconciled by only invoking a warm bias in TEX_{86}. MAAT reconstructions on the other hand have been broadly consistent with nearest living relative based temperature reconstructions on pollen assemblages in many applications in the Eocene (Contreras et al., 2013; Contreras et al., 2014;

Pancost et al., 2013; Pross et al., 2012; Willard et al., 2019), but both brGDGT and plant-based temperature estimates are arguably prone to cold biases at the high-temperature end (e.g. Naafs et al. 2018, Van Dijk et al., 2020). In addition, it may be that the same evolutionary or bacterial community factors that make Paleogene brGDGT assemblages deviate from that in modern soils, may also cause a deviation in the calibration to MAAT. This may resolve some of the offset between MAAT and SST reconstructions. Although this implies that quantitative MAAT estimates based on MBT'$_{5me}$ in non-analogue settings such as the present one should be taken with care, the strong temperature dependence in Paleogene brGDGTs cannot be ignored.

Another surprising result is that the brGDGT-based MAAT record does not capture PETM and MECO warming (Fig. 9c), independent of the calibration chosen. This is remarkable for several reasons: (1) brGDGTs were measured on the same samples as isoGDGTs, which precludes a sampling bias; (2) SST changes of longer duration (Maastrichtian–Danian warming, mid-Paleocene cooling and early Eocene warming towards the EECO) are represented in the MAAT record; (3) The duration of PETM (~150-250 kyrs; Röhl et al., 2007, Zeebe & Lourens, 2019) and MECO (~400 kyrs; Bohaty et al, 2009) is too long to explain the absence in MAAT warming with a lag in soil-derived OM delivery to the ocean (up to several kyr, see, e.g., Feng et al., 2013; Schefuß et al., 2016; Huurdeman et al., 2020); (4) seems incompatible with the fact that other low-amplitude, shorter-term SST changes are reflected in the MAAT record (Fig. 9c, d), which suggests that soil-derived OM did capture short-term climate variability on the time resolution of the samples; (5) Other PETM records in the region do show a temperature response in the PETM in various proxies including brGDGTs (Hollis et al., 2012; Pancost et al., 2013, Huurdeman et al. 2020). A lack of MAAT rise during the PETM and the MECO could be explained by a switch from brGDGT sourcing from soils to (peaty) lakes, which are notoriously cold-biased (Tierney et al., 2010). Paleocene–Eocene peats are abundant in southeast Australia (Holdgate et al., 2009), and it is possible that a contribution from peat lakes at times of global warming, contributed to a dampening of the proxy-response. This may also explain the lack of response at the EECO and explain why MBT'$_{5me}$ does not reach saturation in that interval. The final option, which, although unlikely, cannot be

https://doi.org/10.5194/cp-2021-18
Preprint. Discussion started: 11 March 2021

excluded, is that a dominant fraction of the brGDGT was produced in situ and subdues the temperature response during these warming phases.

The subdued middle-late Eocene cooling in the air temperature record compared to the strong decrease in SST is particularly clear when cross-plotting SST *versus* MAAT (Fig. 9c, d): the relationship between the two proxies is different in the Maastrichtian–early Eocene compared to the middle–late Eocene. This may be related to the start of a progressive northward tectonic drift of the Tasmanian hinterland, which occurred around the same time (Fig. 1). This puts the hinterland of the soil-derived brGDGTs into warmer climate zones throughout the middle–late Eocene, while the ETP remained under influence of the Antarctic-derived Tasman Current (TC) through that time (Huber et al., 2004). The TC cools and likely strengthens in the middle and late Eocene. The terrestrial climate cooled as well, but this signal will be subdued if the soil material is sourced from a progressively lower-latitude environment as Australia drifted northward. Yet, one would expect that the close coupling between land- and seawater temperature in near-shore environments would not capture such tectonic effects.

The correlation between both temperature proxies changes once more during the late Eocene–Oligocene, when they show a sharp cooling of 2–3 °C at the onset of greensand deposition, at ~35.5 Ma. Whereas this is merely a continuation of progressive late Eocene cooling in the SST record, the decrease in MAAT is strongly accelerated compared to middle–late Eocene trends. Another 3–4 °C MAAT drop occurs sometime between the late Eocene and the early Oligocene (likely associated with the Eocene–Oligocene transition), while SSTs returns to warmer, middle Eocene values in this interval. The continued sea surface warmth across the EOT has been related to persistent influence of the proto-Leeuwin Current (Houben et al., 2019), which apparently retained a constant temperature across the EOT. Since MAAT decreased while SSTs remained high, the influence of regional oceanographic changes did not impact climate changes in the source region of brGDGTs during this time interval. This is surprising given the proximity of the sediment record to the coastline.

Minimum mid-Paleocene SSTs are lower than those for the early Oligocene. However, the site migrated northward by ~7 ° of latitude between the mid-Paleocene and the early Oligocene (Fig. 1) and the oceanographic regime changed with throughflow of the proto-Leeuwin Current through the TG in the Late Eocene (Houben et al., 2019). More remarkably, the mid-Paleocene SSTs approach those of the warmest interglacial intervals of Oligocene Wilkes Land Margin, east Antarctica (Hartman et al., 2018), at a similar paleolatitude as the Paleocene ETP. This suggests that mid-Paleocene Antarctic-proximal temperatures were similar to those at times of major Antarctic glaciation during EOT. Previous work has indeed presented widespread evidence for low sea level during this time interval (Frieling et al., 2014; 2018; Guasti et al., 2006; Hollis et al., 2014), which combined with low SSTs suggests the presence of some continental ice on the Antarctic continent during this mid-Paleocene interval.

5.2 BrGMGTs

The continuous presence of brGMGTs in our record appears unrelated to depositional conditions or varying relative contributions of terrestrial material, suggesting that at least part of the brGMGTs have a marine origin. This confirms previous observations from the modern sediments and water column (Liu et al. 2012, Xie et al. 2014) and Paleogene Arctic Ocean sediments (Sluijs et al., 2020). Their sparse presence in modern soils (Peterse et al., pers comm based on metadata from De Jonge et al., 2019; Kirkels et al., 2020) is also in line with this, although abundant occurrence in peats and lakes (Naafs et al., 2018, Baxter et al. 2019, Tang et al., 2021) shows clear potential for terrestrial input. Despite the uncertainties in sourcing of brGMGTs, we find a strong resemblance with the signals from tropical lakes. The brGMGTI, which was derived to quantify the temperature relation of brGMGTs in surface sediments of East African lakes (Baxter et al., 2019), seems to correlate to temperature in our record as well (Fig. 12a–d), although the better correlation of brGMGTI with MAAT than with SST (Fig. 12a–d) seems to be at odds with the presumed marine source of brGMGTs in our record. Despite all potential complications, our study provides additional evidence that a temperature signal may be governing the distribution of the different brGMGT isomers, as proposed by (Baxter et al., 2019), but there are differences as well. For instance, H1020c is altogether absent in the cold mid-Paleocene part of our record. There are numerous ways in which this can be explained, e.g., the biosynthesis of H1020c occurs only above a certain temperature, or the microbes that biosynthesize H1020c do not live at low temperatures, or the site receives brGMGTs from a different catchment in colder climates. Indeed, H1020c was almost absent in the cold (<12°C), high-altitude tropical lake samples (Baxter et al. 2019). However, those cold lakes did have high relative abundance of H1048 (Baxter et al., 2019), which our record lacks in the cold mid-Paleocene, illustrating the differences between modern lakes and our marine depositional setting.

The HMBT record does not reflect a temperature signal when using all brGMGT isomers in the calculation (Fig. 12f), as H1020 isomers are by far the most abundant brGMGTs at Site 1172, and any change in the abundance of H1020c is compensated by both H1020b and H1020a in our record. In contrast, only using the H1020c and H1034b isomers, which following the chromatographic peak identification of Sluijs et al. (2020) match the compounds used to derive the HMBT index based on brGMGTs in peats (Naafs et al., 2018), does show a correlation to temperature in our record (Fig. 12g).

%brGMGT as calculated in Naafs et al., (2018) or as in Baxter et al., (2019) does not show a clear relation with temperature (Fig. 12h, i), in contrast to observations in modern peats (Naafs et al., 2018a) and lake sediments (Baxter et al., 2019). We do note the extremely high %brGMGT (~80%) in the Maastrichtian and Oligocene, much higher than seen anywhere so far. We also do not see a clear inverse relationship between %brGMGT and BIT index, as in Sluijs et al. (2020). This may be because of the complexity in the relative abundance of brGDGTs in the record, which does not necessarily reflect the variation in terrestrial versus marine sourcing.

The higher relative abundance and change in composition of brGMGT composition in the Oligocene that coincides with abundant signs of overprints in all br- and isoGDGT indices may indicate a source change of brGMGTs in this interval, e.g., related to the same changes in contribution that cause the overprints in isoGDGTs. The differences in brGMGT signals between our record, the Eocene Arctic Ocean record and modern sediments demonstrate that more research is needed on their sources and environmental dependencies to further assess their use and value in paleoreconstructions.

5.3 Integrated paleoenvironmental and -climatological reconstruction

5.3.1 Sea level and ecosystem response to SST changes

The abundance of temperature-responsive dinocyst eco-groups qualitatively confirm our SST trends. The thermophile dinocyst eco-group shows higher relative abundance at higher SSTs (Fig. 15). This eco-group has been empirically associated to SST based on its strong affinity to high SST in the global compilation of late Paleocene-early Eocene records (Frieling and Sluijs, 2018), and we here confirm this relationship for the longer early Paleogene. The relationship between isoGDGT-based SSTs and relative abundance of the supposedly cold-affiliated endemic dinocysts (Bijl et al., 2011) is not as clear. This might be because the majority of dinocyst species within the Endemic-Antarctic dinocyst ecogroup are restricted to the Eocene (Bijl et al., 2011).

Indeed, from 50 Ma onwards, SST does have a correlation with the %endemic Antarctic dinocyst abundance in the record (Fig. 15; Bijl et al., 2011), which may indicate a more distinct biogeographical separation through the development of stronger meridional gradients or evolutive adaptation of the endemic dinocyst community to more polar environments following the extreme warmth of the EECO. We particularly note the strong correlation between TEX_{86}-based SST and relative abundance of more open ocean-affiliated dinocysts (Fig. 13), which suggests that SST correlates with regional sea level. SST-induced sea level changes hint at steric effects as driver. Indeed, because of the flatness of continental shelf areas during long-term greenhouse climates (Somme et al., 2009) small changes in regional sea level will cause large changes in distance to shore and associated characteristics, including e.g. salinity, nutrients and suspended sediment loads, which subsequently shapes the dinocyst assemblages.

Fig.15

GDGT- and palynology-based proxies for SST

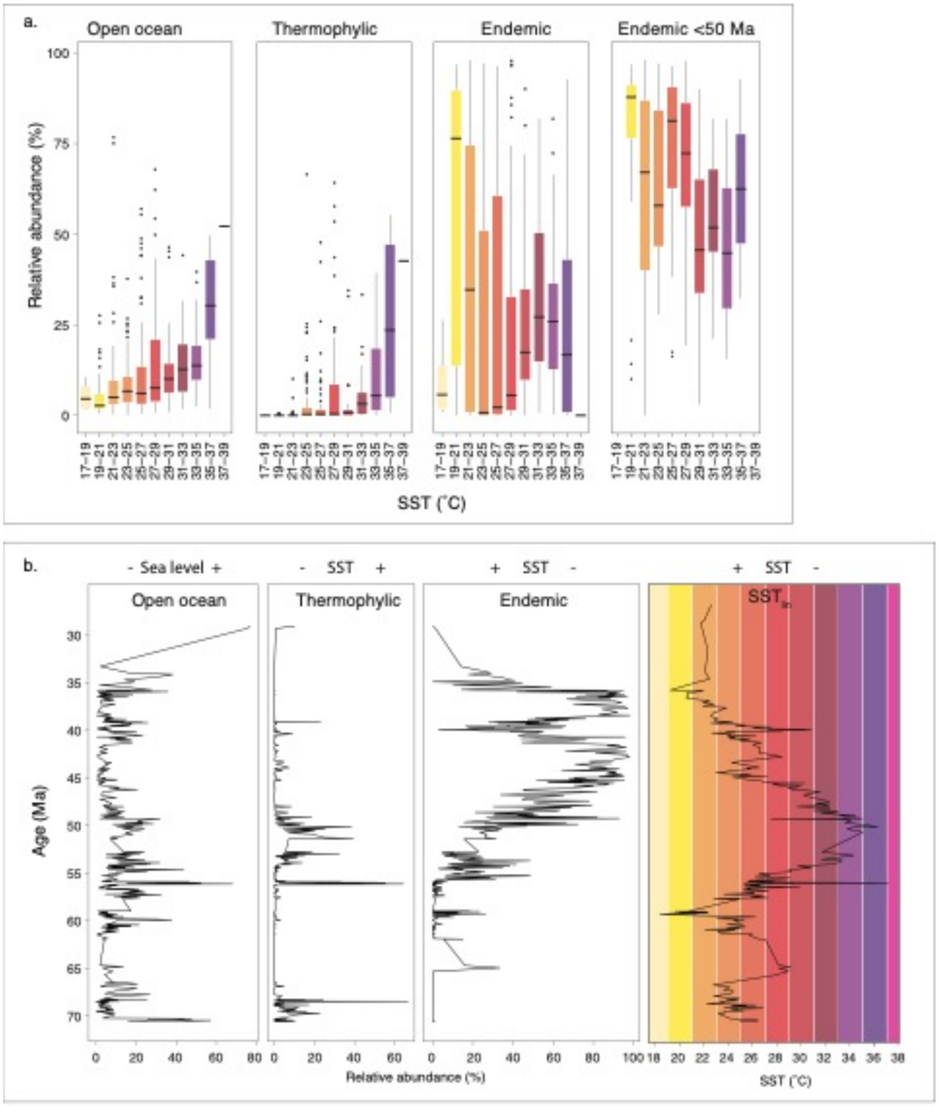

Figure 15. isoGDGT- and palynology-based proxies for SST. a. relative abundance of open ocean, thermophylic and endemic-Antarctic dinocysts (total dataset and samples <50Ma only) plotted against linearly interpolated (resampled) TEX_{86}-based SST, in 2 degree bins. b. Time series of the same dinocyst ecogroups and SST.

The SST control on dinocyst assemblages is further demonstrated in diversity and assemblage variability indices. Throughout the long time interval covered in our record, dinocyst richness and diversity show a remarkably similar pattern to TEX_{86}-based SST. Species richness, as well as diversity expressed in the Shannon and Simpson indices and Fisher's alpha reach a maximum during the prolonged warmth of the EECO and drop during middle–late Eocene cooling. These relationships are demonstrated by modest correlation coefficient between diversity and TEX_{86} (Fig. 13). This pattern holds for the long-term trends, as well as for the short-term PETM, but not for the MECO. Dinocyst diversity is known to vary in an inshore-to-offshore transect in the modern and Eocene (Brinkhuis, 1994; Pross and Brinkhuis, 2005). As our assemblages indeed consist of many mid-shelf species, the strong correlation between diversity and SST might thus be indirectly related through habitat size, with expansion of the flat shelf area and thereby increase in shelf niches during the EECO (Somme et al., 2009). Variability as indicated by the Gibbs index records the opposite pattern to diversity for the long-term trends into and out of the EECO (Fig 14). That is, the lower-diversity assemblages in general have a higher variability, or sample-to-sample fluctuations within the relative abundances. This indicates the higher diversity dinocyst assemblages might be more ecologically resilient.

5.3.2 Marine environmental response to runoff changes

Senegalinium cpx. abundance broadly correlates with the IR (Fig. 16), which signals input of river-produced brGDGTs. *Senegalinium* cpx. is generally thought to have tolerated low salinity environments (Barke et al., 2011; Sluijs et al., 2005; Sluijs and Brinkhuis, 2009). These two proxies together confirm a large input of fresh water at this site during the mid-to-late Paleocene in line with high relative abundance of terrestrial palynomorphs, low abundances of open ocean dinocysts and high IR values (Fig. 16). Interestingly, *Phthanoperidinium* spp., which is also generally associated with low-salinity to near fresh-water conditions (Barke et al., 2011; Frieling and Sluijs, 2018; Sluijs and Brinkhuis, 2009) does not correlate to IR (Fig. 16). Because we find different species of *Phthanoperidinium* spp. than those previously associated to fresh-water conditions (e.g., Barke et al., 2011), it could be that the fresh-water tolerance of *Phthanoperidinium* spp. was not shared among all species. It could also be that *Phthanoperidinium* spp. is slightly less euryhaline than *Senegalinium*.

Tasmania was located at latitudes between 55° and 60° S, in the middle of the region of strong westerly winds, within the range of low atmospheric pressure and received a large amount of precipitation during the Paleocene (Huber and Caballero, 2011). River input from Tasmania and perhaps also Australia could have reached the site. Interestingly, while Tasmania migrated northwards only a few degrees latitude between 60 and 40 Ma (Fig. 1), the freshwater input decreased, based on both *Senegalinium* cpx., terrestrial palynomorph abundance (decimated abundance from 50 Ma onwards) and the IR (decrease to normal values around 54 Ma; Fig. 16). This suggests either a rerouting of river input or a drying of the hinterland. Support for the latter comes from clay mineralogical data, showing an increase in kaolinite starting at 50 Ma (Fig. 2; Robert, 2004). Kaolinite forms abundantly at the base of acidic peats (Staub and Cohen, 1978; Korasidis et al., 2019) and in old, leached soils, which were ubiquitous in the Eocene Australian hinterland (Holdgate et al., 2009). While the hinterland could well retain the kaolinite-rich clays during the Maastrichtian and Paleocene, because the site was under a year-round high precipitation regime, it was less efficient in doing so when the hinterland experienced drier, more variable climatic conditions as Australia migrated northward. The increase in kaolinite delivery to Site 1172 is hence interpreted as a signal of enhanced soil (or peat) erosion from the catchment areas in Tasmania and SW, as a result of a more variable climate regime.

5.4 Environmental and climatological changes in the catchment

The long-term trends in the BIT index are at odds with all the river runoff indicators in our data. BIT remains low during the presumed interval with increased river water discharge, as indicated by the high IR and abundance of *Senegalinium* and increases when this river-input signal ceases. This is unexpected, because the BIT index should reflect high input of soil-derived brGDGTs into the marine sediments, associated with increased discharge (Hopmans et al., 2004). There are two ways to explain this signal. The BIT index could be responding to marine crenarchaeol production, rather than to the terrestrial brGDGT flux. Indeed, marine productivity could have been spurred by runoff and associated nutrient delivery to the coastal zone during the Paleocene, and decreased in the Eocene, affecting BIT index values.

Another explanation is that the BIT index has been influenced by crenarchaeol production in the river (Zell et al., 2013), although the river-produced crenarchaeol concentrations are normally negligible compared to that produced in the marine realm. Decreasing BIT index values with increasing river-and soil input has been related to catchment dynamics in the late Quaternary Zambezi river (Lattaud et al., 2017), involving vegetation dynamics controlling soil-OM input. Studies on modern soil-river-ocean pathways in the Amazon River system show that whereas river-suspended brGDGTs in its upper tributaries reflect catchment soils (Kirkels et al., 2020), brGDGTs in the lower Amazon receive increasing contributions of in situ produced brGDGTs (Zell et al., 2013), and marine surface sediments of the Amazon fan contain a mix of soil, riverine, and marine brGDGTs (Zell et al., 2014). In a high-precipitation, soil-rich environment like the Amazon basin, this can only occur if the river-produced brGDGT production progressively exceeds the soil-derived brGDGTs input in river water along the trajectory of the river, or when the soil-derived brGDGTs are preferentially remineralized during river transport. We here propose the following scenario to explain the BIT index trends: In the Paleocene–early Eocene, excessive, year-round precipitation-fed river runoff caused strong fresh-water delivery into the sw Pacific. Soil-derived brGDGTs were partly remineralized in the river catchment, and the strongly diluted soil-derived OM was dominated by river-produced brGDGTs and crenarchaeol, both in river production and on the continental shelf, which suppressed the BIT index. This explains the unexpectedly cold MAATs derived from the mid-Paleocene samples with high IR. The high riverine input did promote pelagic isoGDGT production: crenarchaeol which decreases the BIT index and isoGDGTs in general. In the early Eocene, precipitation in the hinterland decreased as the hinterland gradually drifted out of the zone of intense precipitation. This reduced river discharge, but at the same time the more dynamic climate regime caused more seasonal precipitation which increased destabilization of Australian and Tasmanian soils, leading to a higher abundance of soil-derived brGDGTs and kaolinite from destabilized soils in the river discharge, and relatively little river-produced brGDGTs (because enhanced soil-OM content increased turbidity) and river-produced crenarchaeol, which increased BIT index at the ETP.

Fig. 16

GDGT- and palynology-based proxies for runoff

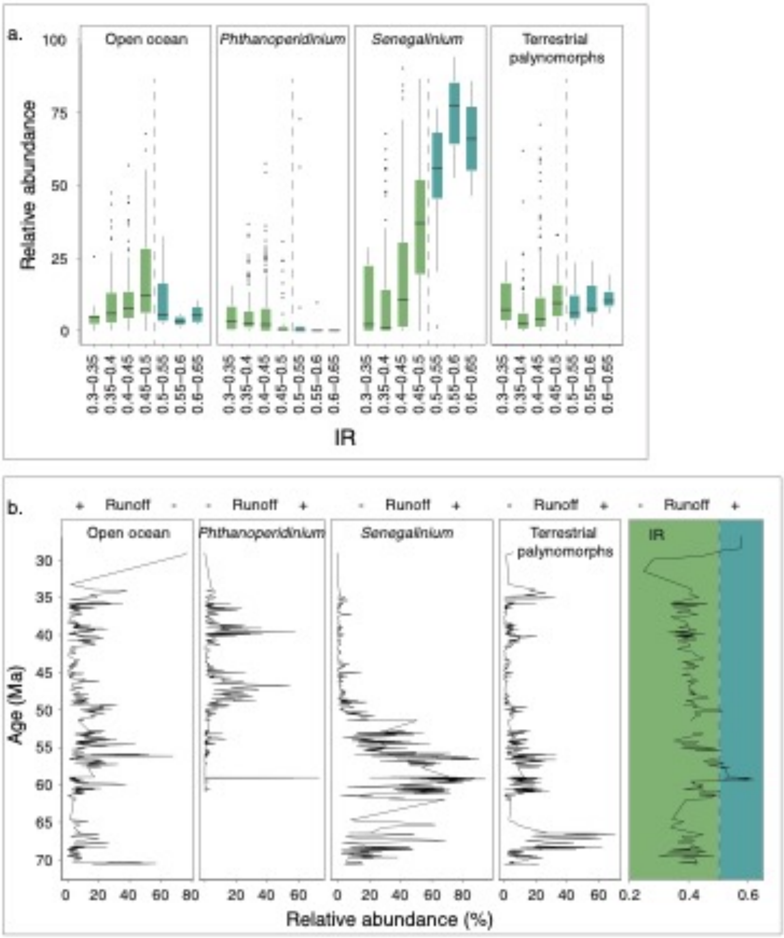

Figure 16. BrGDGT- and palynology-based proxies for river runoff. a. relative abundance of Open Ocean, *Phthanoperidinium* spp., *Senegalinium* cpx. and terrestrial palynomorphs in 0.05 index unit bins of the resampled IR. Dashed line separates elevated IR bins from non-elevated IR bins. b. Time series of the same palynology ecogroups and the IR.

6. Conclusions

We have critically reviewed the GDGT- and dinoflagellate cyst data in samples from the Maastrichtian–lower Oligocene sediments at ODP Site 1172. IsoGDGTs represent a pelagic signal throughout the Maastrichtian–Eocene and are influenced by sedimentary-produced isoGDGTs in the Oligocene. BrGDGTs at our site are likely primarily soil- or peat-derived, albeit evolutionary changes in brGDGT prodcution may have altered the Paleogene soil brGDGT composition. Exceptions are the mid-Paleocene, where river-produced brGDGTs influence the record, and the Oligocene, where marine in situ produced brGDGTs dominate. TEX_{86} and MBT'_{5me} records reveal the SST and MAAT evolution of the region, respectively, consistent with independent existing paleotemperature reconstructions from the same samples. A temperature offset between the SST and MAAT proxies remains poorly reconciled with the coastal proximity of the site but is likely a combined effect of evolutionary differences in MBT'_{5me}-MAAT relationships and a disparate integration of climate signals by both proxies. The subdued air temperature cooling in the middle Eocene compared to the SST cooling could in part reflect progressive northward tectonic drift of the hinterland, while SSTs remained continuously influenced by the Antarctic-derived Tasman Current. Strong MAAT cooling occurred step-wise around the Eocene–Oligocene transition. The absence of SST cooling around the Eocene–Oligocene transition suggests some disconnection between oceanographic reorganisations and regional MAAT changes. The absence of a MAAT response at the PETM and MECO remains unresolved but might be related to shifting sources of brGDGTs during these warm phases.

The relatively high IR, and low $\#rings_{tetra}$ confirm dinocyst assemblages characteristic of an inner mid-shelf depositional setting. We reconstruct strong river-runoff in the Paleocene–early Eocene at this site, and normal open-marine conditions thereafter. The latter reflects a drying and increased seasonality in precipitation in the catchment as the continent tectonically migrates northwards, out of the region of strong precipitation during the middle and late Eocene. The correlation between SST and changes dinoflagellate cyst assemblages and biodiversity metrics suggest temperature-controlled sea level changes influenced the site, probably through steric effects. We find corroborating evidence for a temperature signal in brGMGT assemblages, further demonstrating the potential to develop novel proxies with more extensive studies on modern affinities.

7.Supplements

- Table S1: Age tie points
- Table S2: grouping of dinocysts in ecogroups

8. Data availability

Raw GDGT/GMGT and palynological data presented in this paper, as well as R markdown code for data analysis and visualization can be found on Github (https://github.com/bijlpeter83/RGDGT.git). Data was deposited at zenodo under DOI:10.5281/zenodo.4471204.

9. Author contributions

AS (PETM) and PKB (part) prepared samples for GDGT analyses. PKB (part), AS (PETM) and CB (part) integrated UHPLC-MS results. AS (PETM) and PKB (part) analysed palynological samples. All authors contributed to the interpretation of the OG results, and PKB, AS, JF and MC interpreted dinocyst results. PKB wrote the R script for data analyses and visualization, drafted the figures and wrote the paper with input from all authors.

10. Acknowledgements

This research used samples from the Ocean Drilling Program, which was funded through U.S. National Science foundation under the management of joined oceanographic institutions, inc. We thank Klaas Nierop, Desmond Eefting and Natasja Welters for technical/analytical support. PKB acknowledges funding through NWO Vernieuwingsimpuls Veni grant no. 863.13.002. This work was carried out under the program of the Netherlands Earth System Science Centre (NESSC), financially supported by the Dutch Ministry of Education, Culture and Science. MC and AS thank the Ammodo Foundation for funding unfettered research of laureate AS. PB and AS thank the European Research Council for Starting Grant 802835 OceaNice and Consolidator Grant 771497 SPANC, respectively.

11. References

Anagnostou, E., John, E. H., Edgar, K. M., Foster, G. L., Ridgwell, A., Inglis, G. N., et al.: Changing atmospheric CO_2 concentration was the primary driver of early Cenozoic climate, Nature, 533, 380-384, doi:10.1038/nature17423, 2016.

Barke, J., Abels, H. A., Sangiorgi, F., Greenwood, D. R., Sweet, A. R., Donders, T., et al.: Orbitally forced Azolla blooms and middle Eocene Arctic hydrology: Clues from palynology, Geology, 39, 427-430, 2011.

Baxter, A. J., Hopmans, E. C., Russell, J. M., and Sinninghe Damsté, J. S.: Bacterial GMGTs in east african lake sediments: Their potential as palaeotemperature indicators, Geochimica et Cosmochimica acta 259: 155-169, doi:https://doi.org/10.1016/j.gca.2019.05.039, 2019.

Beerling, D. J., and Royer, D. L.: Convergent Cenozoic CO_2 history, Nature Geoscience, 4, 418-420, 2019.

Bijl, P. K., Bendle, A. P. J., Bohaty, S. M., Pross, J., Schouten, S., Tauxe, L., et al.: Eocene cooling linked to early flow across the Tasmanian Gateway, Proceedings of the National Academy of Sciences of the United States of America 110(24), 9645-9650, 2013a.

Bijl, P. K., Brinkhuis, H., Egger, L. M., Eldrett, J. S., Frieling, J., Grothe, A., et al.: Comment on 'Wetzeliella and its allies–the 'hole' story: A taxonomic revision of the Paleogene dinoflagellate subfamily Wetzelielloideae' by Williams et al. (2015). Palynology, 41(3), 423-429. doi:10.1080/01916122.2016.1235056, 2017.

Bijl, P. K., Houben, A. J. P., Schouten, S., Bohaty, S. M., Sluijs, A., Reichart, G.J., et al.: Transient middle Eocene atmospheric carbon dioxide and temperature variations, Science 330, 819-821, 2010.

Bijl, P. K., Pross, J., Warnaar, J., Stickley, C. E., Huber, M., Guerstein, R., et al.: Environmental forcings of Paleogene Southern Ocean dinoflagellate biogeography, Paleoceanography 26, PA1202, 2011.

Bijl, P. K., Schouten, S., Brinkhuis, H., Sluijs, A., Reichart, G.J., and Zachos, J. C.: Early Palaeogene temperature evolution of the southwest Pacific Ocean, Nature 461, 776-779, 2009.

Bijl, P. K., Sluijs, A., and Brinkhuis, H.: A magneto- chemo- stratigraphically calibrated dinoflagellate cyst zonation of the early Paleogene South Pacific Ocean, Earth-Science Reviews 124, 1-31, 2013b.

Bijl, P. K., Sluijs, A., and Brinkhuis, H.: Erratum to "A magneto- and chemostratigraphically calibrated dinoflagellate cyst zonation of the early Paleogene South Pacific Ocean" [Earth sci. rev. 124 (2013) 1-31], Earth-Science Reviews 134, 160-163. doi:10.1016/j.earscirev.2014.03.010, 2014.

Blaga, C. I., Reichart, G.-J., Heiri, O., and Sinninghe Damsté, J. S.: Tetraether membrane lipid distributions in water-column particulate matter and sediments: A study of 47 European lakes along a north-south transect, Journal of Paleolimnology 41(3), 523-540, doi:10.1007/s10933-008-9242-2, 2009

Bohaty, S. M., Zachos, J. C., and Delaney, M. L.: Foraminiferal Mg/Ca evidence for Southern Ocean cooling across the Eocene–Oligocene transition, EPSL, doi:https://doi.org/10.1016/j.epsl.2011.11.037 ,2012

Bohaty, S. M., Zachos, J. C., Florindo, F., and Delaney, M. L.: Coupled greenhouse warming and deep-sea acidification in the middle Eocene, Paleoceanography 24, doi:10.1029/2008PA001676, 2009

Brinkhuis, H.: Late Eocene to early Oligocene dinoflagellate cysts from the Priabonian type-area (northeast Italy); biostratigraphy and palaeoenvironmental interpretation, Palaeogeography, Palaeoclimatology, Palaeoecology 107, 121-163, 1994.

Brinkhuis, H., Sengers, S., Sluijs, A., Warnaar, J., and Williams, G. L.: Latest Cretaceous to earliest Oligocene, and Quaternary dinoflagellates from ODP site 1172, East Tasman Plateau, In N. Exon, and J. P. Kennett (Eds.), Proceedings of the Ocean Drilling Program, scientific results, volume 189. College Station, Texas: U.S. Government Printing Office, 2003.

Cande, S. C., and Stock, J. M.: Cenozoic reconstructions of the Australia-new Zealand-south Pacific sector of antarctica, In N. F. Exon, J. P. Kennett and M. Malone (Eds.), The Cenozoic Southern Ocean: Tectonics, sedimentation and climate change between australia and Antarctica (pp. 5-18) Geophysical Monograph Series, American Geophysical Union, 2004.

Carpenter, R. J., Jordan, G. J., Macphail, M. K., and Hill, R. S.: Near-tropical early Eocene terrestrial temperatures at the Australo-Antarctic margin, western Tasmania, Geology, 40(3), 267-270, doi:10.1130/G32584.1, 2012

Contreras, L., Pross, J., Bijl, P. K., Koutsodendris, A., Raine, J. I., van de Schootbrugge, B., et al.: Early to middle Eocene vegetation dynamics at the Wilkes Land Margin (Antarctica), Review of Palaeobotany and Palynology 197, 119-142, 2013.

Contreras, L., Pross, J., Bijl, P. K., O'Hara, R. B., Raine, J. I., Sluijs, A., et al.: Southern high-latitude terrestrial climate change during the Palaeocene-Eocene derived from a marine pollen record (ODP site 1172, East Tasman Plateau), Climate of the Past, 10(4), 1401-1420, doi:10.5194/cp-10-1401-2014, 2014.

Cramwinckel, M. J., Huber, M., Kocken, I. J., Agnini, C., Bijl, P. K., Bohaty, S. M., et al.: Synchronous tropical and deep ocean temperature evolution in the Eocene, Nature 559, 382-386, 2018.

Cramwinckel, M. J., Woelders, L., Huurdeman, E. P., Peterse, F., Gallagher, S. J., Pross, J., et al.: Surface-circulation change in the Southern Ocean across the Middle Eocene Climatic Optimum: Inferences from dinoflagellate cysts and biomarker paleothermometry, Climate of the Past, , 1-34, 2020

Creech, J. B., Baker, J. A., Hollis, C. J., Morgans, H. E. G., and Smith, E. G. C.: Eocene sea temperatures for the mid-latitude southwest Pacific from Mg/Ca ratios in planktonic and benthic foraminifera, Earth and Planetary Science Letters, 299, 483-495, 2010.

Crouch, E. M., Shepherd, C. L., Morgans, H. E. G., Naafs, B. D. A., Dallanave, E., Phillips, A., et al.: Climatic and environmental changes across the Early Eocene Climatic Optimum at mid-Waipara River, Canterbury Basin, New Zealand, Earth-Science Reviews, 200, doi:10.1016/j.earscirev.2019.102961, 2020.

Dallanave, E., Bachtadse, V., Crouch, E. M., Tauxe, L., Shepherd, C. L., Morgans, H. E. G., et al.: Constraining early to middle Eocene climate evolution of the southwest Pacific and Southern Ocean. Earth and Planetary Science Letters, 433, 380-392. doi:10.1016/j.epsl.2015.11.010, 2016

De Jonge, C., Hopmans, E. C., Stadnitskaia, A., Rijpstra, W. I. C., Hofland, R., Tegelaar, E., et al.:Identification of novel penta- and hexamethylated branched glycerol dialkyl glycerol tetraethers in peat using HPLC-MS2, GC-MS and GC-SMB-MS, Organic Geochemistry 54, 78-82, doi:10.1016/j.orggeochem.2012.10.004, 2013.

De Jonge, C., Hopmans, E. C., Zell, C. I., Kim, J. -., Schouten, S., and Sinninghe Damsté, J. S.: Occurrence and abundance of 6-methyl branched glycerol dialkyl glycerol tetraethers in soils: Implications for palaeoclimate reconstruction, Geochimica et Cosmochimica Acta, 141, 97-112. doi:10.1016/j.gca.2014.06.013, 2014a.

De Jonge, C., Stadnitskaia, A., Cherkashov, G., and Sinninghe Damsté, J. S.: Branched glycerol dialkyl glycerol tetraethers and crenarchaeol record post-glacial sea level rise and shift in source of terrigenous brGDGTs in the Kara Sea (Arctic Ocean), Organic Geochemistry 92, 42-54, doi:10.1016/j.orggeochem.2015.11.009, 2016.

De Jonge, C., Stadnitskaia, A., Hopmans, E. C., Cherkashov, G., Fedotov, A., and Sinninghe Damsté, J. S.: In situ produced branched glycerol dialkyl glycerol tetraethers in suspended particulate matter from the Yenisei River, eastern Siberia, Geochimica et Cosmochimica Acta, 125, 476-491, doi:10.1016/j.gca.2013.10.031, 2014b.

De Jonge, C., Stadnitskaia, A., Hopmans, E. C., Cherkashov, G., Fedotov, A., Streletskaya, I. D., et al.: Drastic changes in the distribution of branched tetraether lipids in suspended matter and sediments from the Yenisei River and Kara Sea (Siberia): Implications for the use of brGDGT-based proxies in coastal marine sediments, Geochimica et Cosmochimica Acta 165, 200-225, doi:10.1016/j.gca.2015.05.044, 2015.

De Jonge, C., Radujković, D., Sigurdsson, B. D., Weedon, J. T., Janssens, I., and Peterse, F.: Lipid biomarker temperature proxy responds to abrupt shift in the bacterial community composition in geothermally heated soils, Org Geochem, 137, 894 103897, https://doi.org/10.1016/j.orggeochem.2019.07.006, 2019.

Dearing Crampton-Flood, E., Peterse, F., and Sinninghe Damsté, J. S.: Production of branched tetraethers in the marine realm: Svalbard fjord sediments revisited, Organic Geochemistry 138 doi:10.1016/j.orggeochem.2019.103907, 2019.

Dearing Crampton-Flood, E., Tierney, J. E., Peterse, F., Kirkels, F M S A, and Sinninghe Damsté, J. S. BayMBT: A bayesian calibration model for branched glycerol dialkyl glycerol tetraethers in soils and peats, Geochimica Et Cosmochimica Acta, 268, 142-159, doi:10.1016/j.gca.2019.09.043, 2020.

Douglas, P. M. J., Affek, H. P., Ivany, L. C., Houben, A. J. P., Sijp, W. P., Sluijs, A., Schouten, S., Pagani, M.: Pronounced zonal heterogeneity in Eocene southern high latitude sea surface temperatures, PNAS 111 (18), 6582-6587, 2014.

Elling, F. J., K.nneke, M., Lipp, J. S., Becker, K. W., Gagen, E. J., and Hinrichs, K.-U.: Effects of growth phase on the membrane lipid composition of the thaumarchaeon Nitrosopumilus maritimus and their implications for archaeal lipid distributions in the marine environment, Geochim Cosmochim Ac, 141, 579-597, https://doi.org/10.1016/j.gca.2014.07.005, 2014.

Evans, D., Sagoo, N., Renema, W., Cotton, L. J., Müller, W., Todd, J. A., et al.: Eocene greenhouse climate revealed by coupled clumped isotope-Mg/Ca thermometry, Proceedings of the National Academy of Sciences of the United States of America, 115(6), 1174-1179. doi:10.1073/pnas.1714744115, 2018.

Exon, N. F., Kennett, J. P., and Malone, M.: Proceedings of the Ocean Drilling Program, initial reports, volume 189, College Station, Texas: U.S. Government Printing Office., 2001.

Feng, X, Vonk, J.E., van Dongen, B.E., Gustafsson, Ö., Semiletov, I.P., Dudarev, O.V., Wang, Z., Montluçon, D.B., Wacker, L., Eglinton, T.I.: Differential mobilization of terrestrial carbon pools in Eurasian Arctic river basins, PNAS 110 (35) 14168-14173; https://doi.org/10.1073/pnas.1307031110 , 2013.

Fensome, R. A., Taylor, F. J. R., Norris, G., Sarjeant, W. A. S., Wharton, D. I., and Williams, G. L.: In Dinkins G. (Ed.), A classification of modern and fossil dinoflagellates, Salem: Micropalaeontology, Special Paper, 1993.

Fisher, R. A., Corbet, A. S., and Williams, C. B.: The relation between the number of species and the number of individuals in a random sample of an animal population, Journal of Animal Ecology, 12(1), 42-58, doi:10.2307/1411, 1943.

Foster, G. L., Royer, D. L., and Lunt, D. J.: Future climate forcing potentially without precedent in the last 420 million years, Nature Communications, 8, 14845, 2017.

Frieling, J., Gebhardt, H., Huber, M., Adekeye, O. A., Akande, S. O., Reichart, G.J., et al.: Extreme warmth and heat-stressed plankton in the tropics during the Paleocene-Eocene Thermal Maximum. Science Advances, 3(3) doi:10.1126/sciadv.1600891, 2017.

Frieling, J., Huurdeman, E. P., Rem, C. C. M., Donders, T. H., Pross, J., Bohaty, S. M., et al.: Identification of the Paleocene-Eocene boundary in coastal strata in the Otway Basin, Victoria, Australia, Journal of Micropalaeontology, 37(1), 317-339, doi:10.5194/jm-37-317-2018, 2018.

Frieling, J., Iakovleva, A. I., Reichart, G. J., Aleksandrova, G. N., Gnibidenko, Z. N., Schouten, S., et al.: Paleocene–Eocene warming and biotic response in the epicontinental west Siberian Sea, Geology, doi:10.1130/G35724.1, 2014.

Frieling, J., and Sluijs, A.: Towards quantitative environmental reconstructions from ancient non-analogue microfossil assemblages: Ecological preferences of Paleocene – Eocene dinoflagellates, Earth-Science Reviews, 185, 956-973, doi:10.1016/j.earscirev.2018.08.014, 2018.

Fuller, M., and Touchard, Y. On the magnetostratigraphy of the East Tasman Plateau, timing of the opening of the Tasmanian Gateway and paleoenvironmental changes, In N. Exon, J. P. Kennett and M. Malone (Eds.), The Cenozoic Southern Ocean. tectonics, sedimentation and climate change between Australia and Antarctica (pp. 127-151), Washington: American Geophysical Union (AGU) Geophysical Monograph series, 2004.

Gibbs, S. J., Bown, P. R., Murphy, B. H., Sluijs, A., Edgar, K. M., Pälike, H., et al.: Scaled biotic disruption during early Eocene global warming events, Biogeosciences, 9(11), 4679-4688, 2012.

Guasti, E., Speijer, R. P., Brinkhuis, H., Smit, J., and Steurbaut, E.: Paleoenvironmental change at the Danian-Selandian transition in Tunisia: Foraminifera, organic-walled dinoflagellate cyst and calcareous nannofossil records, Marine Micropaleontology, 59, 210-229, 2006.

Hartman, J. D., Bijl, P. K., Sangiorgi, F., Peterse, F., Schouten, S., Salabarnada, A., et al.: Paleoceanography and ice sheet variability offshore Wilkes Land, Antarctica – part 3: Insights from Oligocene–Miocene TEX_{86}-based sea surface temperature reconstructions, Climate of the Past, 14, 1275–1297, 2018.

Hill, P. J., and Exon, N. F.: Tectonics and basin development of the offshore Tasmanian area; incorporating results from deep ocean drilling, In N. F. Exon, J. P. Kennett and M. Malone (Eds.), The Cenozoic Southern Ocean; tectonics, sedimentation and climate change between Australia and Antarctica (Geophysical Monograph

Series 151 ed., pp. 19-19), Washington, D.C., U.S.A.: American Geophysical Union, 2004.

Hill, P. J., and Moore, A. M. G.: Geological framework of the South Tasman Rise and East Tasman Plateau, Geoscience Australia, 2001/40, 2001.

Hines, B. R., Hollis, C. J., Atkins, C. B., Baker, J. A., Morgans, H. E. G., and Strong, P. C.: Reduction of oceanic temperature gradients in the early Eocene southwest Pacific Ocean, Palaeogeography, Palaeoclimatology, Palaeoecology, 475, 41-54, doi:10.1016/j.palaeo.2017.02.037, 2017.

Holdgate, G. R., McGowran, B., Fromhold, T., Wagstaff, B. E., Gallagher, S. J., Wallace, M. W., et al.: Eocene-Miocene carbon-isotope and floral record from brown coal seams in the Gippsland Basin of southeast Australia, Global and Planetary Change, 65(1-2), 89-103, doi:10.1016/j.gloplacha.2008.11.001, 2009

Hollis, C. J., Crouch, E. M., Morgans, H. E. G., Handley, L., Baker, J. A., Creech, J., et al.: Tropical sea temperatures in the high latitude South Pacific during the Eocene, Geology, 37(2), 99-102, 2009.

Hollis, C. J., Dunkley Jones, T., Anagnostou, E., Bijl, P. K., Cramwinckel, M. J., Cui, Y., et al.: The DeepMIP contribution to PMIP4: Methodologies for selection, compilation and analysis of latest paleocene and early Eocene climate proxy data, incorporating version 0.1 of the DeepMIP database, Geoscientific Model Development, 12(7), 3149-3206, doi:10.5194/gmd-12-3149-2019, 2019

Hollis, C. J., Tayler, M. J. S., Andrew, B., Taylor, K. W., Lurcock, P., Bijl, P. K., et al.: Organic-rich sedimentation in the south Pacific Ocean associated with late Paleocene climatic cooling, Earth-Science Reviews, 134, 81-97, 2014.

Hollis, C. J., Taylor, K. W. R., Handley, L., Pancost, R. D., Huber, M., Creech, J. B., et al.: Early Paleogene temperature history of the southwest Pacific Ocean: Reconciling proxies and models, Earth and Planetary Science Letters, 349–350(0), 53-66, doi:10.1016/j.epsl.2012.06.024, 2012

Hopmans, E. C., Schouten, S., and Sinninghe Damsté, J. S.: The effect of improved chromatography on GDGT-based palaeoproxies, Organic Geochemistry, 93, 1-6, doi:10.1016/j.orggeochem.2015.12.006, 2016.

Hopmans, E. C., Weijers, J. W. H., Schefuß, E., Herfort, L., Sinninghe Damsté, J. S., and Schouten, S.: A novel proxy for terrestrial organic matter in sediments based on branched and isoprenoid tetraether lipids, Earth and Planetary Science Letters, 224, 107-116, 2004.

Houben, A. J. P., Bijl, P. K., Sluijs, A., Schouten, S., and Brinkhuis, H.: Late Eocene Southern Ocean cooling and invigoration of circulation preconditioned Antarctica for full-scale glaciation, Geochemistry, Geophysics, Geosystems, 20, https://doi.org/10.1029/2019GC008182, 2019.

Huber, M., Brinkhuis, H., Stickley, C. E., Döös, K., Sluijs, A., Warnaar, J., et al.: Eocene circulation of the Southern Ocean: Was Antarctica kept warm by subtropical waters? Paleoceanography, 19, 4026, 2004.

Huber, M., and Caballero, R.: The early Eocene equable climate problem revisited, Climate of the Past, 7, 603-633, 2011.

Huber, M., and Thomas, E., Paleoceanography: The greenhouse world, in Encyclopedia of Ocean Sciences, pp 319–329, 2010.

Hurley, S. J., Elling, F. J., K.nneke, M., Buchwald, C., Wankel, S. D., Santoro, A. E., Lipp, J. S., Hinrichs, K.-U., and Pearson, A.: Influence of ammonia oxidation rate on thaumarchaeal lipid composition and the TEX86 temperature proxy, Proceedings of the National Academy of Sciences, 113, 7762-7767, 10.1073/pnas.1518534113, 2016.

Huurdeman, E.P., Frieling, J., Reichgelt, T., Bijl, P.K., Bohaty, S.M., Holdgate, G.R., Gallagher, S.J., Peterse, F., Greenwood, D.R., Pross; J.: Rapid expansion of meso-megathermal rain forests into the southern high latitudes at the onset of the Paleocene-Eocene Thermal Maximum. Geology doi: https://doi.org/10.1130/G47343.1, 2020.

Inglis, G. N., Farnsworth, A., Lunt, D., Foster, G. L., Hollis, C. J., Pagani, M., et al.: Descent toward the icehouse: Eocene sea surface cooling inferred from GDGT distributions, Paleoceanography, 30(7), 1000-1020, doi:10.1002/2014PA002723, 2015.

Inglis, G. N., Bragg, F., Burls, N. J., Cramwinckel, M. J., Evans, D., Foster, G. L., Huber, M., Lunt, D. J., Siler, N., Steinig, S., Tierney, J. E., Wilkinson, R., Anagnostou, E., de Boer, A. M., Dunkley Jones, T., Edgar, K. M., Hollis, C. J., Hutchinson, D. K., and Pancost, R. D.: Global mean surface temperature and climate sensitivity of the early Eocene

Climatic Optimum (EECO), Paleocene–Eocene Thermal Maximum (PETM), and latest Paleocene, Clim. Past, 16, 1953–1968, https://doi.org/10.5194/cp-16-1953-2020, 2020.

Kim, J. -., Meer, J. v. d., Schouten, S., Helmke, P., Willmott, V., Sangiorgi, F., et al.: New indices and calibrations derived from the distribution of crenarchaeal isoprenoid tetraether lipids: Implications for past sea surface temperature reconstructions, Geochimica et Cosmochimica Acta, 74, 4639-4654, 2010.

Kirkels, F. M. S. A., Ponton, C., Galy, V., West, A. J., Feakins, S. J., and Peterse, F.: From Andes to Amazon: Assessing Branched Tetraether Lipids as Tracers for Soil Organic Carbon in the Madre de Dios River System, Journal of Geophysical Research: Biogeosciences, 125, e2019JG005270, 10.1029/2019jg005270, 2020.

Korasidis, V. A., Wallace, M. W., Dickinson, J. A., and Hoffman, N.: Depositional setting for Eocene seat earths and related facies of the Gippsland Basin, Australia, Sedimentary Geology, doi:10.1016/j.sedgeo.2019.07.007, 2019

Kozdon, R., Penman, D. E., Kelly, D. C., Zachos, J. C., Fournelle, J. H., & Valley, J. W.: Enhanced poleward flux of atmospheric moisture to the Weddell Sea region (ODP Site 690) during the Paleocene-Eocene Thermal Maximum, Paleoceanography and Paleoclimatology, 35, e2019PA003811, https://doi.org/10.1029/2019PA003811 , 2020

Lattaud, J., Dorhout, D., Schulz, H., Castañeda, I. S., Schefuß, E., Damsté, J. S. S., et al.: The C32 alkane-1,15-diol as a proxy of late Quaternary riverine input in coastal margins, Climate of the Past, 13(8), 1049-1061, doi:10.5194/cp-13-1049-2017, 2017.

Lauretano, V., Zachos, J. C., and Lourens, L. J.: Orbitally paced carbon and deep-sea temperature changes at the peak of the Early Eocene Climatic Optimum. Paleoceanography and Paleoclimatology, 33(10), 1050-1065, doi:10.1029/2018PA003422, 2018.

Leutert, T. J., Auderset, A., Martínez-García, A., Modestou, S., and Meckler, A. N.: Southern Ocean temperature evolution coupled to middle Miocene ice sheet expansion, Nature Geoscience 13, 634-639, 2020.

Liu, X., Lipp, J. S., Simpson, J. H., Lin, Y., Summons, R. E., and Hinrichs, K.: Mono- and dihydroxyl glycerol dibiphytanyl glycerol tetraethers in marine sediments: Identification of both core and intact polar lipid forms. Geochimica et Cosmochimica Acta, 89, 102-115. doi:https://doi.org/10.1016/j.gca.2012.04.053, 2012.

Lunt, D. J., Jones, T. D., Heinemann, M., Huber, M., LeGrande, A., Winguth, A., et al.: A model-data comparison for a multi-model ensemble of early Eocene atmosphere-ocean simulations: EoMIP, Climate of the Past, 8(5), 1717-1736, 2012.

Lunt, D. J., Bragg, F., Chan, W.-L., Hutchinson, D. K., Ladant, J.-B., Morozova, P., Niezgodzki, I., Steinig, S., Zhang, Z., Zhu, J., Abe-Ouchi, A., Anagnostou, E., de Boer, A. M., Coxall, H. K., Donnadieu, Y., Foster, G., Inglis, G. N., Knorr, G., Langebroek, P. M., Lear, C. H., Lohmann, G., Poulsen, C. J., Sepulchre, P., Tierney, J. E., Valdes, P. J., Volodin, E. M., Dunkley Jones, T., Hollis, C. J., Huber, M., and Otto-Bliesner, B. L.:

DeepMIP: model intercomparison of early Eocene climatic optimum (EECO) large-scale climate features and comparison with proxy data, Clim. Past, 17, 203–227, https://doi.org/10.5194/cp-17-203-2021, 2021.

Macphail, M. K.: Australian palaeoclimates, cretaceous to tertiary, volume 1: Review of palaeobotanical and related evidence up to 2000, Canberra: Geology Department, Australian National University, 2000.

Macphail, M. K.: ODP Leg 189 initial results: Terrestrial plant microfossils. Canberra: Geoscience Australia, 2002

Mertens, K. N., Dale, B., Ellegaard, M., Jansson, I. -., Godhe, A., Kremp, A., et al.: Process length variation in cysts of the dinoflagellate protoceratium reticulatum, from surface sediments of the baltic-kattegat-skagerrak estuarine system: A regional salinity proxy, Boreas, 40(2), 242-255, 2011

Moore, D. H., Betts, P. G., and Hall, M.: Towards understanding the early Gondwanan margin in southeastern Australia, Gondwana Research, 23(4), 1581-1598, doi:10.1016/j.gr.2012.08.006, 2013.

Müller, R. D., Gaina, C., and Clark, S.: Seafloor spreading around Australia, In J. Veevers (Ed.), Billion-year earth history of Australia and neighbours in gondwanaland (2000) – BYEHA (pp. 1-1) School of Geosciences, University of Sydney, 2000

Naafs, B. D. A., Gallego-Sala, A. V., Inglis, G. N., and Pancost, R. D.: Refining the global branched glycerol dialkyl glycerol tetraether (brGDGT) soil temperature calibration, Organic Geochemistry, 106, 48-56, doi:10.1016/j.orggeochem.2017.01.009, 2017.

Naafs, B. D. A., Inglis, G. N., Blewett, J., McClymont, E. L., Lauretano, V., Xie, S., et al.: The potential of biomarker proxies to trace climate, vegetation, and biogeochemical processes in peat: A review, Global and Planetary Change, 179, 57-79, doi:10.1016/j.gloplacha.2019.05.006, 2019.

Naafs, B. D. A., Inglis, G. N., Zheng, Y., Amesbury, M. J., Biester, H., Bindler, R., et al.: Introducing global peat-specific temperature and pH calibrations based on brGDGT bacterial lipids, Geochimica et Cosmochimica Acta, 208, 285-301, doi:10.1016/j.gca.2017.01.038, 2017.

Naafs, B. D. A., McCormick, D., Inglis, G. N., and Pancost, R. D.: Archaeal and bacterial H-GDGTs are abundant in peat and their relative abundance is positively correlated with temperature, Geochimica Et Cosmochimica Acta, 227, 156-170, doi:10.1016/j.gca.2018.02.025, 2018.

Naafs, B. D. A., Rohrssen, M., Inglis, G. N., Lähteenoja, O., Feakins, S. J., Collinson, M. E., et al.: High temperatures in the terrestrial mid-latitudes during the early Palaeogene, Nature Geoscience, 11(10), 766-771, doi:10.1038/s41561-018-0199-0, 2018.

O'Brien, C. L., Robinson, S. A., Pancost, R. D., Sinninghe Damsté, J. S., Schouten, S., Lunt, D. J., et al.: Cretaceous sea-surface temperature evolution: Constraints from TEX_{86} and planktonic foraminiferal oxygen isotopes, Earth-Science Reviews, 172, 224-247, doi:10.1016/j.earscirev.2017.07.012, 2017.

O'Brien, C. L., Huber, M., Thomas, E., Pagani, M., Super, J. R., Elder, L. E., et al.: The enigma of Oligocene climate and global surface temperature evolution, Proceedings of the National Academy of Sciences, 202003914, doi:10.1073/pnas.2003914117, 2020.

O'Connor, L. K., Robinson, S. A., Naafs, B. D. A., Jenkyns, H. C., Henson, S., Clarke, M., et al.: Late Cretaceous temperature evolution of the southern high latitudes: A TEX_{86} perspective, Paleoceanography and Paleoclimatology, 34(4), 436-454, doi:10.1029/2018PA003546, 2019.

Oksanen, J., Blanchet, F. G., Friendly, M., Kindt, R., Legendre, P., McGlinn, D., et al.: Vegan: Community ecology package, 2015.

Pancost, R. D., Taylor, K. W. R., Inglis, G. N., Kennedy, E. M., Handley, L., Hollis, C. J., et al.: Early Paleogene evolution of terrestrial climate in the SW Pacific, southern New Zealand, Geochemistry, Geophysics, Geosystems, 14(12), 5413-5429, 2013.

Passchier, S., Bohaty, S. M., Jiménez-Espejo, F., Pross, J., Röhl, U., Van De Flierdt, T., et al.: Early Eocene to middle Miocene cooling and aridification of east Antarctica, Geochemistry, Geophysics, Geosystems, 14(5), 1399-1410, 2013

Passchier, S., Ciarletta, D. J., Miriagos, T. E., Bijl, P. K., and Bohaty, S. M.: An Antarctic stratigraphic record of stepwise ice growth through the Eocene-Oligocene transition, Bulletin of the Geological Society of America, 129(3-4), 318-330, doi:10.1130/B31482.1, 2017.

Peterse, F., Kim, J. -., Schouten, S., Kristensen, D. K., Koç, N., and Sinninghe Damsté, J. S.: Constraints on the application of the MBT-CBT paleothermometer at high latitude environments (Svalbard, Norway), Organic Geochemistry, 40, 692-699, 2009.

Peterse, F., Meer, J. v. d., Schouten, S., Weijers, J. W. H., Fierer, N., Jackson, R. B., et al.: Revised calibration of the MBT-CBT paleotemperature proxy based on branched tetraether membrane lipids in surface soils. Geochimica Et Cosmochimica Acta, 2012.

Pross, J., & Brinkhuis, H., Organic-walled dinoflagellate cysts as paleoenvironmental indicators in the paleogene; a synopsis of concepts, Palaeontologische Zeitschrift, Band 79, 53-59, 2005.

Pross, J., Contreras, L., Bijl, P. K., Greenwood, D. R., Bohaty, S. M., Schouten, S., et al.: Persistent near-tropical warmth on the Antarctic continent during the early Eocene epoch, Nature, 488, 73-73, 2012.

Qin, W., Carlson, L. T., Armbrust, E. V., Devol, A. H., Moffett, J. W., Stahl, D. A., and Ingalls, A. E.: Confounding effects of oxygen and temperature on the TEX_{86} signature of marine Thaumarchaeota, Proceedings of the National Academy of Sciences, 112, 10979-10984, 10.1073/pnas.1501568112, 2015.

Reichgelt, T., West, C.K., Greenwood, D.R.: The relation between global palm distribution and climate, Scientific Reports 8(1), DOI: 10.1038/s41598-018-23147-2, 2018.

Robert, C.: Cenozoic environments in the Tasmanian area of the Southern Ocean (ODP Leg 189): Inferences from bulk and clay mineralogy, Geophysical Monograph Series, 151, 127-151, 2004.

Rochon, A., Lewis, J., Ellegaard, M., and Harding, I. C.: The gonyaulax spinifera (dinophyceae) “complex”: Perpetuating the paradox? Review of Palaeobotany and Palynology, 155(1), 52-60, doi:https://doi.org/10.1016/j.revpalbo.2008.12.017, 2008.

Röhl, U., Brinkhuis, H., Stickley, C. E., Fuller, M., Schellenberg, S. A., Wefer, G., et al.: Sea level and astronomically induced environmental changes in middle and late Eocene sediments from the East Tasman Plateau. Geophysical Monograph Series, 151, 127-151, 2004a.

Röhl, U., Brinkhuis, H., Sluijs, A., and Fuller, M.: On the search for the Paleocene/eocene boundary in the Southern Ocean: Exploring ODP Leg 189 Holes 1171D and 1172D, Tasman Sea, Geophysical Monograph Series, 151, 113-124, 2004b.

Röhl, U., Westerhold, T., Bralower, T. J., and Zachos, J. C.: On the duration of the Paleocene-Eocene Thermal Maximum (PETM), Geochemistry, Geophysics, Geosystems, 8, Q12002, 2007.

Salamy, K.A., Zachos, J.C.: Latest Eocene-Early Oligocene climate change and Southern Ocean fertility: Inferences from sediment accumulation and stable isotope data, Palaeogeogr., Palaeoclimatol., Palaeoecol. 145, 61–77, 1999.

Schefuß, E., Eglinton, T., Spencer-Jones, C. et al.: Hydrologic control of carbon cycling and aged carbon discharge in the Congo River basin, Nature Geosciences 9, 687–690, 2016.

Schellenberg, S. A., Brinkhuis, H., Stickley, C. E., Fuller, M., Kyte, F. T., and Williams, G. L.: The Cretaceous/Paleogene transition on the East Tasman Plateau, southwestern Pacific, In N. Exon, J. P. Kennett and M. Malone (Eds.), The Cenozoic Southern Ocean; tectonics, sedimentation and climate change between Australia and Antarctica (pp. 93-112), Washington: Geophysical Monograph Series, 2004.

Schouten, S., Hopmans, E. C., Schefuß, E., and Sinninghe Damsté, J. S.: Distributional variations in marine crenarchaeotal membrane lipids: A new tool for reconstructing ancient sea water temperatures? Earth and Planetary Science Letters, 204, 265-274, 2002.

Schouten, S., Hopmans, E. C., and Sinninghe Damsté, J. S., The organic geochemistry of glycerol dialkyl glycerol tetraether lipids: A review, Organic Geochemistry, 54, 19-61, doi:10.1016/j.orggeochem.2012.09.006, 2013.

Seton, M., Müller, R. D., Zahirovic, S., Gaina, C., Torsvik, T., Shephard, G., et al.: Global continental and ocean basin reconstructions since 200 Ma, Earth-Science Reviews, 113(3-4), 212-270, 2012.

Shannon, C. E.: A mathematical theory of communication, Bell System Technical Journal, 27(3), 379-423, doi:10.1002/j.1538-7305.1948.tb01338.x, 1948.

Sijp, W. P., Von Der Heydt, A S, and Bijl, P. K.: Model simulations of early westward flow across the Tasman Gateway during the early Eocene, Climate of the Past, 12(4), 807-817, doi:10.5194/cp-12-807-2016, 2016.

Sijp, W. P., von der Heydt, A S, Dijkstra, H. A., Flögel, S., Douglas, P. M. J., and Bijl, P. K.: The role of ocean gateways on cooling climate on long time scales, Global and Planetary Change, 119, 1-22, doi:10.1016/j.gloplacha.2014.04.004, 2014.

Simpson, E.: Measurement of diversity. Nature, 163, 688, 1949.

Sinninghe Damsté, J. S.: Spatial heterogeneity of sources of branched tetraethers in shelf systems: The geochemistry of tetraethers in the Berau River delta (Kalimantan, Indonesia), Geochimica et Cosmochimica Acta, 186, 13-31, doi:10.1016/j.gca.2016.04.033, 2016.

Sluijs, A., Schouten, S., Pagani, M., Woltering, M., Brinkhuis, H., Sinninghe Damsté, J. S., et al.: Subtropical Arctic Ocean temperatures during the Palaeocene/Eocene Thermal Maximum, Nature, 441, 610-613, 2006.

Sluijs, A., Bijl, P. K., Schouten, S., Röhl, U., Reichart, G.J., and Brinkhuis, H.: Southern Ocean warming and hydrological change during the Paleocene-Eocene Thermal Maximum, Climate of the Past, 7, 47-61, 2011.

Sluijs, A., and Brinkhuis, H.: A dynamic climate and ecosystem state during the Paleocene-Eocene Thermal Maximum: Inferences from dinoflagellate cyst assemblages on the New Jersey Shelf, Biogeosciences, 6(8), 1755-1781, 2009.

Sluijs, A., Brinkhuis, H., Stickley, C. E., Warnaar, J., Williams, G. L., and Fuller, M.: Dinoflagellate cysts from the Eocene - Oligocene transition in the Southern Ocean: Results from ODP Leg 189, In N. Exon, and J. P. Kennett (Eds.), Proceedings of the Ocean Drilling Program, scientific results, volume 189, College Station, Texas: U.S. Government Printing Office, 2003.

Sluijs, A., Frieling, J., Inglis, G. N., Nierop, K. G. J., Peterse, F., Sangiorgi, F., et al.: Late Paleocene – early Eocene Arctic Ocean sea surface temperatures; reassessing biomarker paleothermometry at lomonosov ridge, Clim. Past Discuss., doi:rg/10.5194/cp-2020-13, 2020.

Sluijs, A., Pross, J., and Brinkhuis, H.: From greenhouse to icehouse; organic walled dinoflagellate cysts as paleoenvironmental indicators in the Paleogene, Earth-Science Reviews, 68, 281-315, 2005.

Sluijs, A., van Roij, L., Harrington, G. J., Schouten, S., Sessa, J. A., LeVay, L. J., et al.: Warming, euxinia and sea level rise during the Paleocene–Eocene Thermal Maximum on the Gulf Coastal plain: Implications for ocean oxygenation and nutrient cycling, Climate of the Past, 10(4), 1421-1439, doi:10.5194/cp-10-1421-2014, 2014.

Somme, T. O., Helland-Hansen, W., and Granjeon, D., Impact of eustatic amplitude variations on shelf morphology, sediment dispersal, and sequence stratigraphic interpretation: Icehouse versus greenhouse systems, Geology, 37(7), 587-590, 2009.

Staub, J.R., Cohen, A.D.: Kaolinite-enrichment Beneath Coals; A Modern Analog, Snuggedy Swamp, South Carolina, SEPM J Sediment Res Vol. 48(1):203–210, 1978.

Stickley, C. E., Brinkhuis, H., McGonigal, K. L., Chapronière, G. C. H., Fuller, M., Kelly, D. C., et al.: Late Cretaceous - Quaternary biomagnetostratigraphy of ODP Site 1168, 1170, 1171 and 1172, Tasmanian Gateway, In N. F. Exon, J. P. Kennett and M. J. Malone (Eds.), Proceedings of the Ocean Drilling Program, scientific results, volume 189, 2004a.

Stickley, C. E., Brinkhuis, H., Schellenberg, S. A., Sluijs, A., Röhl, U., Fuller, M., et al.: Timing and nature of the deepening of the Tasmanian Gateway, Paleoceanography, 19, 4027, 2004b.

Tang, X., Naafs, B. D., Pancost, R. D., Liu, Z., Fan, T., & Zheng, Y.: Exploring the influences of temperature on "H-shaped" glycerol dialkyl glycerol tetraethers in a stratigraphic context: Evidence from two peat cores across the late Quaternary, Frontiers in Earth Science, 8, 477, 2021.

Taylor, K. W. R., Huber, M., Hollis, C. J., Hernandez-Sanchez, M. T., and Pancost, R. D.: Re-evaluating modern and Palaeogene GDGT distributions: Implications for SST reconstructions, Global and Planetary Change, 108, 158-174, 2013.

Thomas, D. J., Bralower, T. J., and Jones, C. E.: Neodymium isotopic reconstruction of the late Paleocene - early Eocene thermohaline circulation, Earth and Planetary Science Letters, 209(3-4), 309-322, 2003.

Thomas, D. J., Korty, R., Huber, M., Schubert, J. A., and Haines, B.: Nd isotopic structure of the Pacific Ocean 70–30 Ma and numerical evidence for vigorous ocean circulation and ocean heat transport in a greenhouse world, Paleoceanography, PA2535, 2014.

Tierney, J. E., and Russell, J. M.: Distributions of branched GDGTs in a tropical lake system: Implications for lacustrine application of the MBT/CBT paleoproxy, doi:10.1016/j.orggeochem.2009.04.014, 2009.

Tierney, J. E., Sinninghe Damsté, J. S., Pancost, R. D., Sluijs, A., and Zachos, J. C.: Eocene temperature gradients, Nature Geoscience, 10(8), 538-539, doi:10.1038/ngeo2997, 2017.

Tierney, J. E., and Tingley, M. P.: A TEX_{86} surface sediment database and extended bayesian calibration, Scientific Data, 2 doi:10.1038/sdata.2015.29, 2015.

Tierney, J. E., & Tingley, M. P.: BAYSPLINE: A new calibration for the alkenone paleothermometer, Paleoceanography and Paleoclimatology, 33(3), 281-301, doi:10.1002/2017PA003201, 2018.

Torsvik, T. H., Van der Voo, R., Preeden, U., Niocaill, C. M., Steinberger, B., Doubrovine, P. V., et al.: Phanerozoic polar wander, palaeogeography and dynamics, Earth-Science Reviews, 114(3-4), 325-368, 2012.

Truswell, E. M.: Palynomorph assemblages from marine Eocene sediments on the west Tasmanian continental margin and the South Tasman Rise. Australian Journal of Earth Sciences, 44, 633-654, 1997.

Van Dijk, J., Fernandez, A., Bernasconi, S.M., Caves Rugenstein, J.K., Passey, S.R., White, T.: Spatial pattern of super-greenhouse warmth controlled by elevated specific humidity, Nature Geoscience, 13 (11), pp. 739-744, 2020.

Van Hinsbergen, D. J. J., De Groot, L. V., Van Schaik, S. J., Spakman, W., Bijl, P. K., Sluijs, A., et al.: A paleolatitude calculator for paleoclimate studies, PLoS ONE, 10(6), 2015.

Warden, L., Kim, J. -., Zell, C., Vis, G. -., De Stigter, H., Bonnin, J., et al.: Examining the provenance of branched GDGTs in the tagus river drainage basin and its outflow into the Atlantic Ocean over the holocene to determine their usefulness for paleoclimate applications, Biogeosciences, 13(20), 5719-5738, doi:10.5194/bg-13-5719-2016, 2016.

Warden, L., Moros, M., Weber, Y., and Sinninghe Damsté, J. S.: Change in provenance of branched glycerol dialkyl glycerol tetraethers over the Holocene in the Baltic Sea and its impact on continental climate reconstruction, Organic Geochemistry, 121, 138-154, doi:10.1016/j.orggeochem.2018.03.007, 2018.

Warnaar, J., Bijl, P. K., Huber, M., Sloan, L. C., Brinkhuis, H., Röhl, U., et al.: Orbitally forced climate changes in the Tasman sector during the middle Eocene, Palaeogeography, Palaeoclimatology, Palaeoecology, 280, 361-370, 2009.

Weijers, J. W. H., Lim, K. L. H., Aquilina, A., Damsté, J. S. S., and Pancost, R. D.: Biogeochemical controls on glycerol dialkyl glycerol tetraether lipid distributions in sediments characterized by diffusive methane flux, Geochemistry, Geophysics, Geosystems, 12(10), doi:10.1029/2011GC003724, 2011.

Weijers, J. W. H., Schouten, S., Spaargaren, O. C., and Sinninghe Damste, J. S.: Occurrence and distribution of tetraether membrane lipids in soils: Implications for the use of the TEX_{86} proxy and the BIT index, Organic Geochemistry, 37, 1680-1693, 2006.

Weijers, J. W. H., Schouten, S., van den Donker, J C, Hopmans, E. C., and Sinninghe Damsté, J. S.: Environmental controls on bacterial tetraether membrane lipid distribution in soils, Geochimica Et Cosmochimica Acta, 71, 703-713, 2007.

Westerhold, T., Marwan, N., Drury, A. J., Liebrand, D., Agnini, C., Anagnostou, E., et al.: An astronomically dated record of earth's climate and its predictability over the last 66 million years. Science, 369(6509), 1383-1387, doi:10.1126/science.aba6853, 2020.

Willard, D. A., Donders, T. H., Reichgelt, T., Greenwood, D. R., Sangiorgi, F., Peterse, F., et al.: Arctic vegetation, temperature, and hydrology during early Eocene transient global warming events, Global and Planetary Change, 178, 139-152, doi:10.1016/j.gloplacha.2019.04.012, 2019.

Williams, G. L., Fensome, R. A., and MacRae, R. A.: Dinoflaj3, American Association of Stratigraphic Palynologists, Data Series, 2, 2017.

Williams, S. E., Whittaker, J. M., Halpin, J. A., and Müller, R. D.: Australian-Antarctic breakup and seafloor spreading: Balancing geological and geophysical constraints, Earth-Science Reviews, 188, 41-58, doi:10.1016/j.earscirev.2018.10.011, 2019

Xie, S., Liu, X., Schubotz, F., Wakeham, S. G., & Hinrichs, K.: Distribution of glycerol ether lipids in the oxygen minimum zone of the eastern tropical north pacific ocean, Organic Geochemistry, 71, 60-71, doi:https://doi.org/10.1016/j.orggeochem.2014.04.006, 2014.

Zachos, J. C., Schouten, S., Bohaty, S., Quattlebaum, T., Sluijs, A., Brinkhuis, H., et al.: Extreme warming of mid-latitude coastal ocean during the Paleocene-Eocene Thermal Maximum: Inferences from TEX and isotope data, Geology, 34(9), 737-740, 2006.

Zeebe, R.E., Lourens, L.J.: Solar System chaos and the Paleocene–Eocene boundary age constrained by geology and astronomy, Science, 365 (6456), pp. 926-929, 2019.

Zell, C., Kim, J. -., Dorhout, D., Baas, M., and Sinninghe Damsté, J. S.: Sources and distributions of branched tetraether lipids and crenarchaeol along the Portuguese continental margin: Implications for the BIT index, Continental Shelf Research, 96, 34-44, doi:10.1016/j.csr.2015.01.006, 2015.

Zell, C., Kim, J. -., Hollander, D., Lorenzoni, L., Baker, P., Silva, C. G., et al.: Sources and distributions of branched and isoprenoid tetraether lipids on the Amazon shelf and fan: Implications for the use of GDGT-based proxies in marine sediments, Geochimica et Cosmochimica Acta, 139, 293-312, doi:10.1016/j.gca.2014.04.038, 2014.

Zell, C., Kim, J. -., Moreira-Turcq, P., Abril, G., Hopmans, E. C., Bonnet, M. -., et al.: Disentangling the origins of branched tetraether lipids and crenarchaeol in the lower Amazon River: Implications for GDGT-based proxies, Limnology and Oceanography, 58(1), 343-353, doi:10.4319/lo.2013.58.1.0343, 2013

Zhang, Y. G., Pagani, M., and Wang, Z.: Ring index: A new strategy to evaluate the integrity of TEX_{86} paleothermometry, Paleoceanography, 31(2), 220-232, doi:10.1002/2015PA002848, 2016.

Zhang, Y. G., Zhang, C. L., Liu, X. -., Li, L., Hinrichs, K. -., and Noakes, J. E.: Methane index: A tetraether archaeal lipid biomarker indicator for detecting the instability of marine gas hydrates, Earth and Planetary Science Letters, 307(3-4), 525-534, doi:10.1016/j.epsl.2011.05.031, 2011.